NAVAL POSTGRADUATE SCHOOL

MONTEREY, CALIFORNIA

THESIS

FRICTION STIR PROCESSING OF NICKEL ALUMINUM PROPELLER BRONZE IN COMPARISON TO FUSION WELDS

by

David L. Murray

June 2005

Thesis Advisor: Terry R. McNelley

Approved for public release; distribution is unlimited

THIS PAGE INTENTIONALLY LEFT BLANK

REPORT DOCUMENTATION PAGE			*Form Approved OMB No. 0704-0188*
Public reporting burden for this collection of information is estimated to average 1 hour per response, including the time for reviewing instruction, searching existing data sources, gathering and maintaining the data needed, and completing and reviewing the collection of information. Send comments regarding this burden estimate or any other aspect of this collection of information, including suggestions for reducing this burden, to Washington headquarters Services, Directorate for Information Operations and Reports, 1215 Jefferson Davis Highway, Suite 1204, Arlington, VA 22202-4302, and to the Office of Management and Budget, Paperwork Reduction Project (0704-0188) Washington DC 20503.			
1. AGENCY USE ONLY *(Leave blank)*	**2. REPORT DATE** June 2005	**3. REPORT TYPE AND DATES COVERED** Master's Thesis	
4. TITLE AND SUBTITLE: Friction Stir Processing of Nickel-Aluminum Propeller Bronze in Comparison to Fusion Welds			**5. FUNDING NUMBERS**
6. AUTHOR(S) Murray, David L			
7. PERFORMING ORGANIZATION NAME(S) AND ADDRESS(ES) Naval Postgraduate School Monterey, CA 93943-5000			**8. PERFORMING ORGANIZATION REPORT NUMBER**
9. SPONSORING /MONITORING AGENCY NAME(S) AND ADDRESS(ES) Defense Advanced Research Project Agency (DARPA): Dr. Leo Christodoulou DARPA/DSO, 3701 North Fairfax Drive, Arlington, VA 22203-1714			**10. SPONSORING/MONITORING AGENCY REPORT NUMBER**
11. SUPPLEMENTARY NOTES The views expressed in this thesis are those of the author and do not reflect the official policy or position of the Department of Defense or the U.S. Government.			
12a. DISTRIBUTION / AVAILABILITY STATEMENT Approved for public release; distribution is unlimited			**12b. DISTRIBUTION CODE**

13. ABSTRACT (maximum 200 words)

Friction Stir Processing (FSP) is currently being considered for use in manufacture of the Navy's NiAl bronze propellers. Incorporating this technology may improve service performance and enable reduction of manufacturing time and cost. This program of research has employed miniature tensile sample designs to examine the distributions of longitudinal properties through the various regimes in a fusion weld. Also, the distributions of both longitudinal and transverse properties throughout the stir zones for selected FSP conditions were examined. Yield strengths were larger in various FSP conditions by at least a factor of two relative to fusion welds. Ultimate strengths were comparable in the weld pool and stir nugget. Widmanstätten microstructures and microvoid formation and coalescence in the fracture surface resulted in high ductilities in weld metal and the stir nugget. The thermomechanically affected zone of FSP and the heat affected zone of a fusion weld both exhibit low ductility. This may reflect formation of β upon heating to temperatures of 800-850°C, followed by rapid cooling and transformation of the β to form martensitic transformation products in their respective microstructures. For a single-pass raster pattern, transverse ductility is lower than longitudinal ductility. For a multi-pass raster, transverse ductility is higher than longitudinal ductility. For multi-pass raster and spiral patterns in FSP, the data show that the mechanical properties are more nearly isotropic.

14. SUBJECT TERMS Friction Stir Processing, Ni Al Bronze, Microstructure, Mechanical Properties			**15. NUMBER OF PAGES** 91
			16. PRICE CODE
17. SECURITY CLASSIFICATION OF REPORT Unclassified	**18. SECURITY CLASSIFICATION OF THIS PAGE** Unclassified	**19. SECURITY CLASSIFICATION OF ABSTRACT** Unclassified	**20. LIMITATION OF ABSTRACT** UL

NSN 7540-01-280-5500 Standard Form 298 (Rev. 2-89)
Prescribed by ANSI Std. 239-18

THIS PAGE INTENTIONALLY LEFT BLANK

Approved for public release; distribution is unlimited

FRICTION STIR PROCESSING OF NICKEL ALUMINUM PROPELLER BRONZE IN COMPARISON TO FUSION WELDS

David L. Murray
Lieutenant, United States Navy
B.S., The Ohio State University, 1998

Submitted in partial fulfillment of the
requirements for the degree of

MASTER OF SCIENCE IN MECHANICAL ENGINEERING

from the

NAVAL POSTGRADUATE SCHOOL
June 2005

Author: David L. Murray

Approved by: Terry McNelley
Thesis Advisor

Anthony J. Healey
Chairman
Department of Mechanical and Astronautical Engineering

THIS PAGE INTENTIONALLY LEFT BLANK

ABSTRACT

Friction Stir Processing (FSP) is currently being considered for use in manufacture of the Navy's NiAl bronze propellers. Incorporating this technology may improve service performance and enable reduction of manufacturing time and cost. This program of research has employed miniature tensile sample designs to examine the distributions of longitudinal properties through the various regimes in a fusion weld. Also, the distributions of both longitudinal and transverse properties throughout the stir zones for selected FSP conditions were examined. Yield strengths were larger in various FSP conditions by at least a factor of two relative to fusion welds. Ultimate strengths were comparable in the weld pool and stir nugget. Widmanstätten microstructures and microvoid formation and coalescence in the fracture surface resulted in high ductilities in weld metal and the stir nugget. The thermomechanically affected zone of FSP and the heat affected zone of a fusion weld both exhibit low ductility. This may reflect formation of β upon heating to temperatures of 800-850°C, followed by rapid cooling and transformation of the β to form martensitic transformation products in their respective microstructures. For a single-pass raster pattern, transverse ductility is lower than longitudinal ductility. For a multi-pass raster, transverse ductility is higher than longitudinal ductility. For multi-pass raster and spiral patterns in FSP, the data show that the mechanical properties are more nearly isotropic.

THIS PAGE INTENTIONALLY LEFT BLANK

TABLE OF CONTENTS

LIST OF FIGURES

THIS PAGE INTENTIONALLY LEFT BLANK

LIST OF TABLES

THIS PAGE INTENTIONALLY LEFT BLANK

ACKNOWLEDGMENTS

The author would like to thank the Defense Advanced Research Projects Agency and Dr. Leo Christodoulou for support of this research, Mr. Murray Mahoney and his personnel at the Rockwell Scientific Center, Thousand Oaks, CA, as well as Mr. Bill Palko, Dr. David Forrest and Jennifer Nguyen at Naval Surface Warfare Center-Carderock Division for their material support

Special thanks to Professor Terry McNelley for his insights, support and unyielding patience. It was a pleasure working for you.

Thanks to Dr. Alex Zhilyaev, Dr. Keiichiro Oh-Ishi and Dr. Chanman Park for all of your support. I always believe that the evidence of someone understanding concepts means that someone can explain it, no matter what language is most familiar to you. All of you did that very well and I am very grateful to have met all of you.

I would also like to thank LT Frank Pierce, USCG for restoring the Charmilles Andrew EF630 electric discharge machine (EDM) and LCDR Rob Williams for providing essential information facilitating the completion of my thesis.

I would also like to thank Stephanie Mattson, Doug Aelm and many others at Instron for their prompt customer service. It is greatly appreciated.

I would like to thank my family, especially my mother and father, and my friends, professors and colleagues for providing support for me. It is too many names to list here, since I need to leave plenty of room for my thesis.

Last, but certainly first, I would like to thank the Lord for allowing me to put everything in his hands. Experience shows that my hands are just not good enough.

THIS PAGE INTENTIONALLY LEFT BLANK

I. INTRODUCTION

A. OVERVIEW

Useful combinations of the mechanical properties of strength, ductility and toughness have been long desired in materials for structural applications, and are obtainable to varying degrees through numerous processing methods. Friction Stir Processing (FSP) is a relatively new technology that provides for the improvement of mechanical properties in selected locations by modifying the microstructure within a layer near the surface of the material. Moreover, the improvement in mechanical properties is obtained without macroscopic deformation of the material. In a program funded by the Defense Advanced Research Projects Agency, the research being conducted at the Naval Postgraduate School in collaboration with other program participants intends to provide a correlation between the microstructure and mechanical properties in various materials. Moreover, the program will establish the foundation necessary to facilitate the commercialization of FSP, and the specific techniques to be utilized in the post processing of U.S. Navy propeller castings. A thorough understanding of the mechanical and microstructural properties in relation to thermomechanical history as well as just thermal history, and with respect to process parameters, is essential for meeting this objective.

B. FRICTION STIR PROCESSING

Friction stir processing (FSP) is a new metal working technology that can provide localized modification and control of microstructures in near-surface layers of processed metallic components [1-3]. FSP utilizes the same basic methodology as friction stir welding (FSW). FSW is a solid state joining process invented at The Welding Institute (TWI) in 1991 initially as a technique for joining Al alloys that are troublesome to fusion weld [4]. FSP modifies local microstructures in a single material workpiece in the absence of joining. A schematic illustration of FSP is shown in Figure 1. In FSP, a specially designed, cylindrical tool is rotated and plunged into a selected location on the workpiece surface, as shown in Figure 1a. The tool has a small diameter pin with a concentric, larger diameter shoulder. When plunged into the material, the rotating pin

contacts the surface, causing frictional and adiabatic heating as the metal deforms plastically at high rates. This is shown in Figure 1b. The tool shoulder and pin length control the penetration depth, as indicated in Figure 1c. Large areas can be processed by traversing the tool in a pattern on the surface of the workpiece, as suggested in Figure 1d.

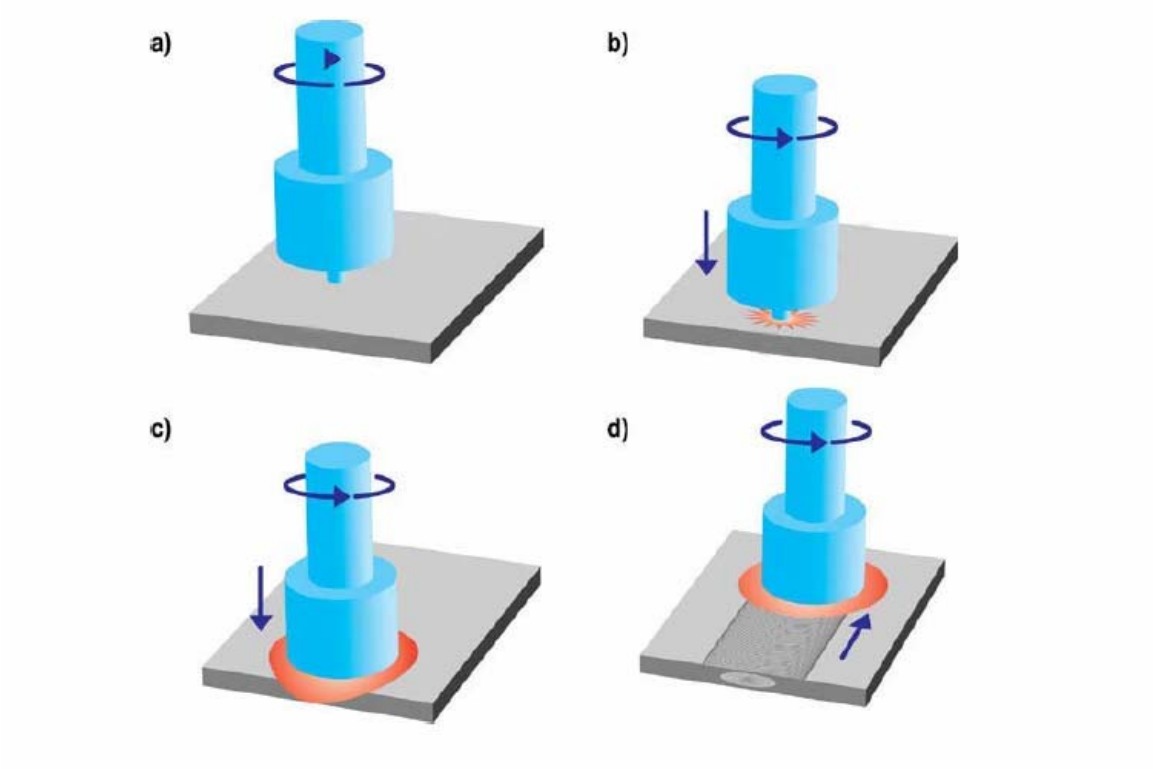

Figure 1. Schematic illustration of FSP (After 4).

FSP is a hot working process involving extreme localized strains and strain rates, as well as high temperatures, and is capable of transforming microstructure and mechanical properties of cast material to a wrought condition. This will result in significant increases in the properties of both strength and toughness [5, 6]. The process is also characterized by steep gradients in strain, strain rate and temperature, resulting in corresponding gradients in both microstructure and mechanical properties. Secondary benefits for some materials include superplasticity effects, better weldability and improved fatigue/corrosion resistance [7]. It is important to note that the improvement in mechanical properties and its corresponding microstructures occur without melting the material. At locations near the surface of the material, peak temperatures (T_{peak}) reach > 0.9 T_{melt} but melting or solidification products have not been observed.

FSP parameters and material conditions are defined with terminology related to

that used in welding. In common with welding processes, FSP has a regime where a reduction in mechanical properties occurs. Fusion welds have a "heat affected zone" (HAZ), and in FSP, there is also a thermomechanically affected zone (TMAZ) where localized hotworking occurs involving only relatively small deformations [6]. The region unique to FSP is the "stir zone" (SZ), also known as the "stir nugget" [4-7] in which both severe plastic deformation and adiabatic heating take place. The micrograph in Figure 2 shows a transverse section of FSP NiAl Bronze. This figure depicts three important zones. They are the SZ, TMAZ and HAZ, relative to the base metal, from the middle of the material proceeding outwards toward base metal.

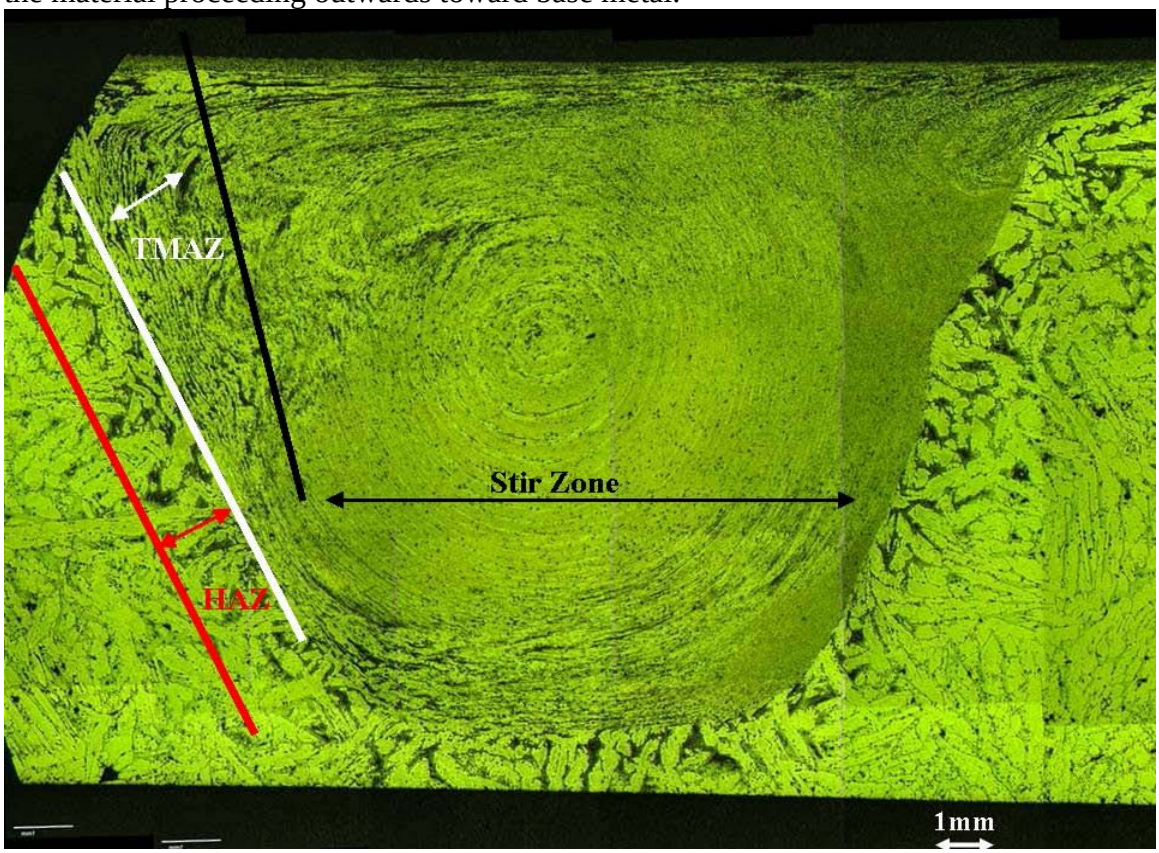

Figure 2. Example of the FSP Zone. (From 8).

The diameter of the tool shoulder can vary from several millimeters to several centimeters. Scroll-shaped grooves on the shoulder surface in contact with the workpiece have been employed in our effort to enhance material flow. Pin depths for these tools can range up to 100% of their largest diameter, depending on the material. The pin is always concentric to the shoulder, but includes thread or step-spiral patterns to induce flow metal in the SZ. The tool geometry is an important parameter in determining the size and shape

of the SZ and its corresponding TMAZ and HAZ regions. The speed of rotation is an adjustable parameter and is generally expressed in revolutions per minute (RPM). The travel direction is defined as the direction the rotational axis of the tool travels and is not restricted to straight lines. The speed, or traverse rate, of the tool is expressed as inches per minute (IPM). The axial force is applied inline of the rotational axis and nearly normal to the surface of the material; the alignment mismatch is because the tool axis may be inclined away from the travel direction to minimize the amount of residual defects.

FSP can be used to process large areas by using linear, raster or spiral traversing patterns. An example of raster and spiral patterns is shown in the schematic in Figure 3. These schematics show the tool (in a plan view) and the sense of tool rotation (which remains fixed during processing. The FSP process is not symmetric about the line of traverse. On the advancing side, the traversing and tangential velocities are added, where on the retreating side, the traversing and tangential velocities are subtracted.

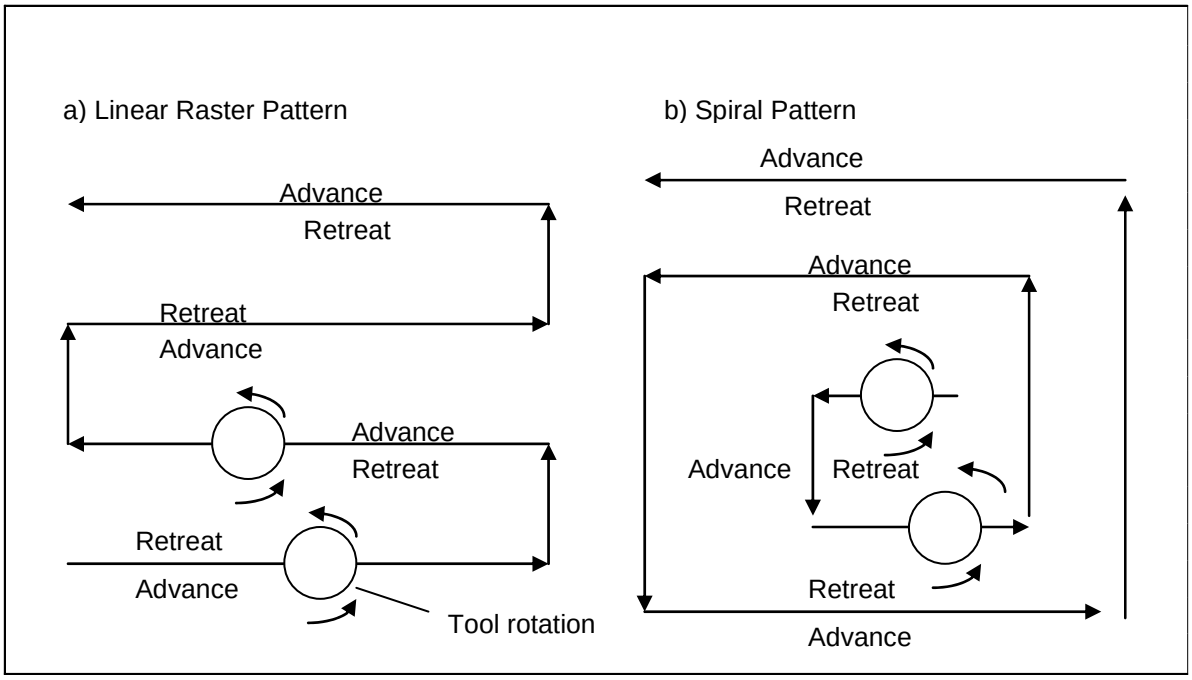

Figure 3. Example of Linear Raster Pattern and Spiral Pattern in Friction Stir Processing. Linear rasters have advance/advance and retreating/retreating passes, whereas spiral patterns have an overlapping of advancing and retreating sides, improving the likelihood of isotropy.

Microstructures within the FSP material are significantly different from the advancing to the retreating side of the stir zone. On the advancing side, where tool rotation direction and travel direction are the same, the microstructure is typically very fine and homogeneous. On the retreating side, where tool rotation is opposite the travel direction, the microstructure is not as refined and thus, inhomogeneous. The effects of advancing and retreating sides are reduced when transitioning from using a linear pass to linear rasters and spiral patterns. Moreover, the use of the spiral pattern is good for potentially ensuring the isotropy of mechanical properties and corresponding microstructures within the stir zone due to the overlay of advancing and retreating sides.

C. NICKEL ALUMINUM BRONZE

Nickel-aluminum bronze (NAB), which, for certain compositions, is also known as "propeller bronze," gained its popularity for marine applications because it exhibits a unique combination of properties that include moderate strength and toughness coupled with excellent fatigue, corrosion, cavitation and erosion resistance [9-10]. Propeller bronzes are Copper (Cu) based alloys with additions of Aluminum (Al), Nickel (Ni), Iron (Fe) and Manganese (Mn). Percentages of the alloying elements can vary, but fall under the specification ASTM B 148-78 designation C95800 [11]. Ship propeller castings and the casting process itself lowers the overall values of the mechanical properties when compared with wrought material primarily due to large casting sizes. Propeller castings require many months of post-cast processing to render the propellers fit for service [12]. The massively thick sections in propeller casts result in very slow cooling rates [13]. Temperature gradients are shallow and cooling times from pouring temperatures to ambient temperature are often more than one week, which correspond to cooling rates of 10^{-3} C° /s. Investigations into the effects of slow cooling in propeller casts have shown that degradation in properties can be directly attributed to related phase changes in conjunction with grain coarsening [9, 13]. Heat treatments have been attempted to mitigate the phase structure changes and segregation effects. In general, heat treatments can alter the material microstructure to obtain more desirable properties. However, the aforementioned heat treatments do not remove other casting defects, particularly porosity [9, 13]. The treatments themselves have also been noted to promote an overall decrease

in ductility [9]. Surface and sub-surface porosity remains an issue and is currently repaired with costly inspection, weld repair and re-inspection processes. Welding repairs to alleviate the effects of porosity currently use an area welding technique known as "buttering" that can potentially introduce undesirable thermal stresses and corresponding microstructural changes [12]. This repetitive method for cast porosity repair leads to leads to times up to 18 months in propeller fabrication. In comparison, FSP can be applied using a rastering method than can be conducted to selectively treat localized regions where an improvement in mechanical properties is desired. A robotic machine used in propeller manufacture is illustrated in Figure 4. In addition to the improvements in mechanical property, another advantage of friction stir processing is the elimination of the repetitive repair process associated with closing porosity. Moreover, FSP has been projected to lower post-cast processing time as well as lower cost associated with the ability to continue to use cast products, versus wrought products.

Figure 4. Area Processing of a Marine Propeller (From 14). The robotic machine from NSWC Carderock is used to manufacture propeller. A spiral pattern is shown on the propeller.

1. NAB Microstructure

The four primary microstructures associated with the friction stir processing of NAB are pictured below in Figure 5. Microstructures within and surrounding the SZ are lamellar (Figure 5a), fine grain (Figure 5b), Widmanstätten (Figure 5c) and as-cast (Figure 5d).

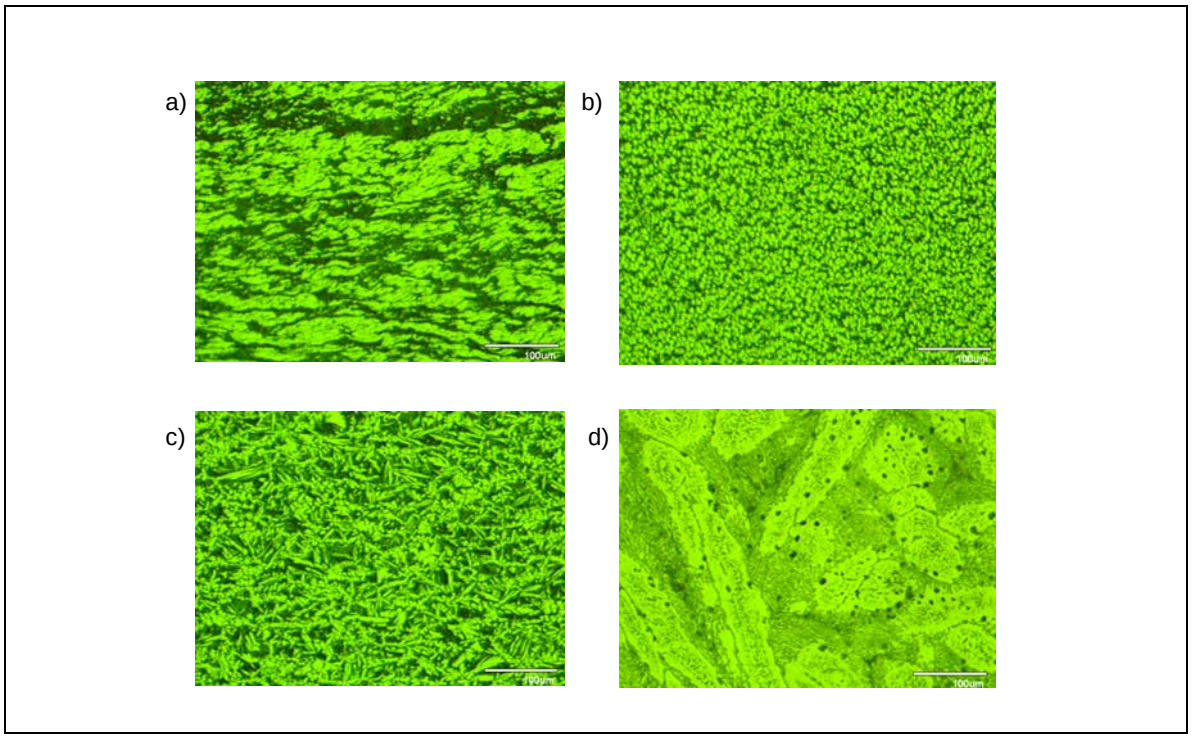

Figure 5. Microstructures created in NAB by friction stir processing.

D. PREVIOUS FINDINGS

Previous mechanical and microstructural studies have analyzed phase transformations and used isothermal hot rolling to provide estimates of FSP temperature and deformation effects. The results of these studies are the building blocks of this research. McNelley and Oh-Ishi [15] have demonstrated that FSP generates peak temperatures of 930-1000°C based on the various transformation products at different locations in the SZ of processed material. Moreover, they [16] illustrated that the Widmanstätten microstructure is associated with high volume fraction of β and this generally provides high tensile ductility. Pierce [17] showed that annealing a material

alone does not provide the improvements of both strength and ductility. Pierce's work show that the benefits of higher temps exceeding 950°C and its associated high strains include involving strong and ductile Widmanstätten microstructures, as well as corresponding improvements of ductility, as shown in Figure 6. Also, as the rolling strain is increased, temperatures exceeding 950°C exhibited the best combination of mechanical properties involving the yield strength, ultimate tensile strength and ductility.

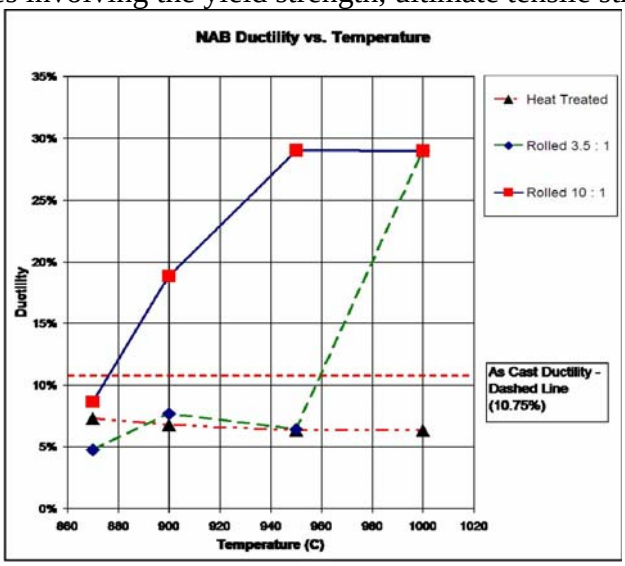

Figure 6. Ductility vs. Temperature Graph (From 17).

An essential component to this unique effect is the linear increase with temperature of high-strength prior β transformation products for heating between approximately 800 ^{0}C and 1000 ^{0}C. This strengthening effect of these constituents is contrary to the effects of ordinary heat treating in which an increase in temperature is associated with softening and a corresponding loss in strength.

Williams [8] demonstrated that the use of single-pass and multi-pass raster processes further enhances microstructural refinement, when compared to linear processes. However, areas of low ductility were still associated with composite microstructures involving the TMAZ and/or HAZ at the periphery of the SZ. A comparison of mechanical properties and microstructures between conventional welds and FSP will enable isolation of thermal effects from thermomechanical effects on the mechanical properties.

E. OBJECTIVE

An objective of this research is to correlate the mechanical properties with the various microstructures of NAB undergoing conventional weld repair using a fusion weld, ie, gas metal arc welding, in the longitudinal direction. An investigation of the HAZ in conventional weld repairs is necessary to observe any evidence of areas of low ductility. An underlying question is: Can a manufacturer subject the same design constraints in a friction stir processed material as one would in a material that has experienced weld repair using conventional methods? Another objective is to correlate the mechanical properties with the various microstructures of Friction Stir Processed NAB utilizing a single-pass and multi-pass FSP involving a raster pattern in the transverse direction and compare to longitudinal data obtained previously by Williams. Areas of low ductility in FSP NAB are of particular interest in this research. Another objective in this research is the correlation of mechanical properties with the various microstructures of FSP NAB using a spiral pattern in both the longitudinal and transverse direction and again, comparing to the properties observed in Fusion Weld NAB.

THIS PAGE INTENTIONALLY LEFT BLANK

II. EXPERIMENTAL PROCEDURES AND TESTING

A. TENSILE TESTING

1. Sample Preparation

Miniature tensile samples were sectioned from base material, weld metal or stir processed material using a Charmilles Andrew EF630 electric discharge machine (EDM) employing consumable brass cutting wire with a nominal diameter of 0.30 mm. The advantage of using the EDM over sawing or abrasive cutting is the ability for the machine to cut the complex geometries without imparting large external forces or excessive heat which may adversely affect the quality and accuracy of the tensile specimens. Moreover, the EDM minimized the amount of waste material. This allowed for maximizing the amount of test material used from the available usable volume. The precision of the EDM machine facilitated the tight control of the cutting lines and improved the accuracy of the tensile testing results.

Each blank was cut individually and numbered prior to sectioning. Each tensile sample was numbered and indexed as it was sectioned from its respective blank. Each tensile sample was surfaced using the Buehler ECOMET 4 polishing wheel by sanding all surfaces up to 4000 grit using 400 grit, 1000 grit, 2400 grit and 4000 grit SiC paper. Flatness of the tensile specimens was ensured prior to mechanical testing. The tensile specimens were then examined using optical and stereo microscopy to examine for macro defects, ie., cracks, voids, etc., which could potentially affect the results of mechanical testing. The initial sample dimensions are included in Figure 7, and were according to ASTM E-8 standards (18). The small size of these samples relative to the size of weld metal deposits or stir zones enables the spatial variations in strength and ductility to be resolved by mechanical testing.

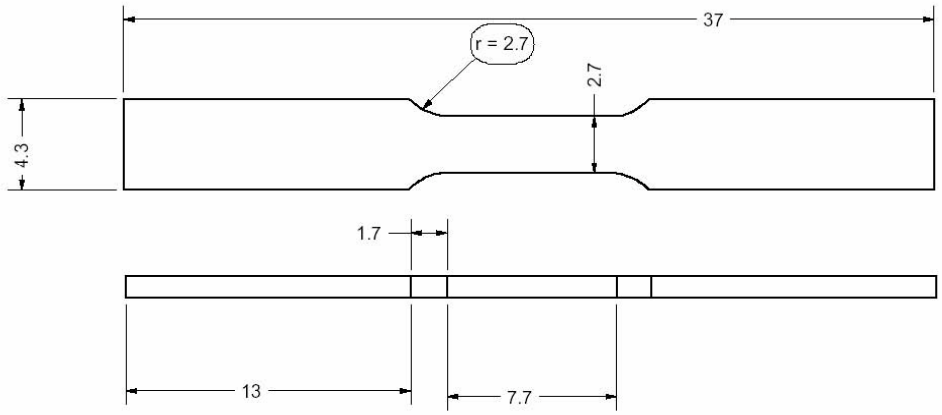

Figure 7. Initial Miniature Tensile Specimen Geometry (From 20). All dimensions are in mm. The presence of strain hardening outside of the gage length resulted in the necessity of a different tensile specimen geometry to ensure that deformation takes place only within the gage length.

The sample indexing was similar to that developed by Williams. (8). Due to the amount of plastic deformation that occurred outside of the gage length when testing the fusion welded NAB material, a new tensile specimen geometry was developed to ensure that deformation took place only within the gage length, and is shown in Figure 8. The revised tensile geometry was also in accordance with ASTM E-8 for sub-size specimen (18). In particular, the gage length was increased from 7.7 mm to 15.9 mm and the gage width was reduced from 2.7 mm. to 1.7 mm. Moreover, the overall length of the tensile specimen was increased from 37.1 mm to 59.5 mm to ensure that more of the grips were utilized and improve the reliability of the results obtained from tensile testing. All data in this research involved mechanical property comparisons from the same sample geometry.

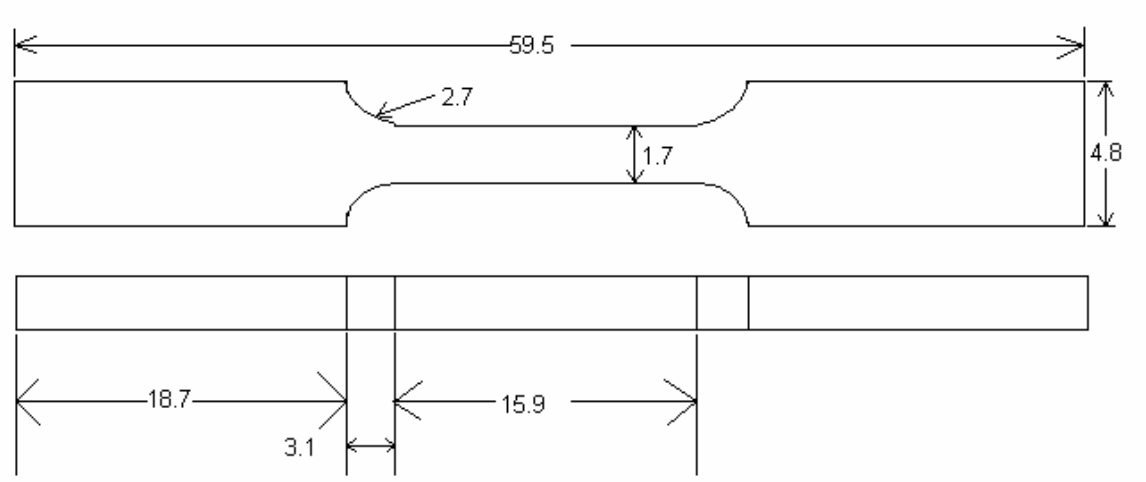

Figure 8. Revised Miniature Tensile Specimen Geometry, where all dimensions are in mm. This geometry facilitated the improved accuracy in mechanical testing.

Each 1mm sample was numbered sequentially beginning at the plate surface and continuing through the depth. The purpose of utilizing sub-size tensile specimen was to minimize the microstructural gradients that would be present in a larger tensile specimen.

2. Mechanical Testing

The computer controlled INSTRON Model 4507 with GPIB interface control and the Series IX data collection software was used to perform all tensile testing. Due to the aforementioned grinding of the tensile specimen, the gage width and gage thickness was measured prior to loading the tensile specimen. Using a standard tensile test method with a constant cross head displacement speed, the specimens were loaded to failure. Great care was exercised to properly align all samples through the centerline of the grips as they were mounted into the screw platen grips. Moreover, a metal rectangular block was utilized to help ensure consistent sample alignment. A universal joint was also added between the load cell and the upper grip to aid in tensile load alignment. Prior to each test, the load cell and extension length were reset, balanced and calibrated at the INSTRON control panel. Also, the gage width and thickness was entered prior to each test. During each run, engineering stress, engineering strain, load cell and crosshead

displacement data were gathered at 5 Hz and recorded in an ASCII 2 formatted file. Once the data were recorded, a locally prepared MATLAB m-file using MATLAB Version 6.5 was used to import the data. The aforementioned MATLAB m-file was used to compensate for the elastic response due to the machine frame and grips. This was necessary due to the inability to use an extensometer when testing the mini-samples. A typical set of stress-strain plots is shown in Figure 9.

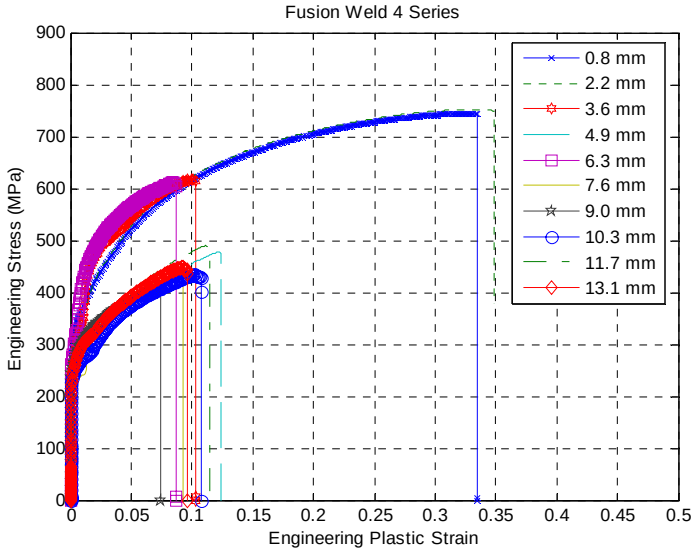

Figure 9. Stress-strain plots with revised tensile geometry, where the depth below the surface is indicated. The stress-strain curve is for a fusion weld, where the ductility was highest in the weld pool near the surface and lowest in regions associated with the heat affected zone (6.3 mm), followed by corresponding increases in ductility in base metal.

An observation from Figure 9 is that some tensile specimens using the design in Figure 7 exhibited anomalous double yielding. This double yielding phenomenon resulted from a high strain hardening rate in the gage section and thus yielding outside of the gage region after an initial strain interval. This necessitated the design of a tensile specimen with a thinner and longer gage length, as previously shown in Figure 8. Another observation that was noticed for all specimen tested was that little or no necking was noticeable once the ultimate tensile strengths were achieved.

B. MATERIAL & COMPOSITION

Friction Stir Processed material shown in Figure 10 was provided by Rockwell Scientific Corporation [19]. Fusion welding was accomplished at the Naval Surface Warfare Center (NSWC)-Carderock Division [20]. A groove of rectangular cross section, 16 mm in width and 6 mm in depth, was filled with a weld deposit. A total of six passes were made using Amptrode 46 filler wire, gas-metal arc processes and operation at 24.5 V, 239 amps. The chemical analyses for 740, 741 and 751 FSP materials were obtained from ANAMET Laboratories Inc., in Hayward, CA. Composition data was provided for the fusion weld plate by NSWC-Carderock Division. Composition data was provided by Rockwell Scientific Corporation for the 1398 FSP plate. The accepted nominal composition, composition data for material used in previous research, Alloy 1 and Alloy 2 [21], and the data for material used in the current research are contained in Table 1.

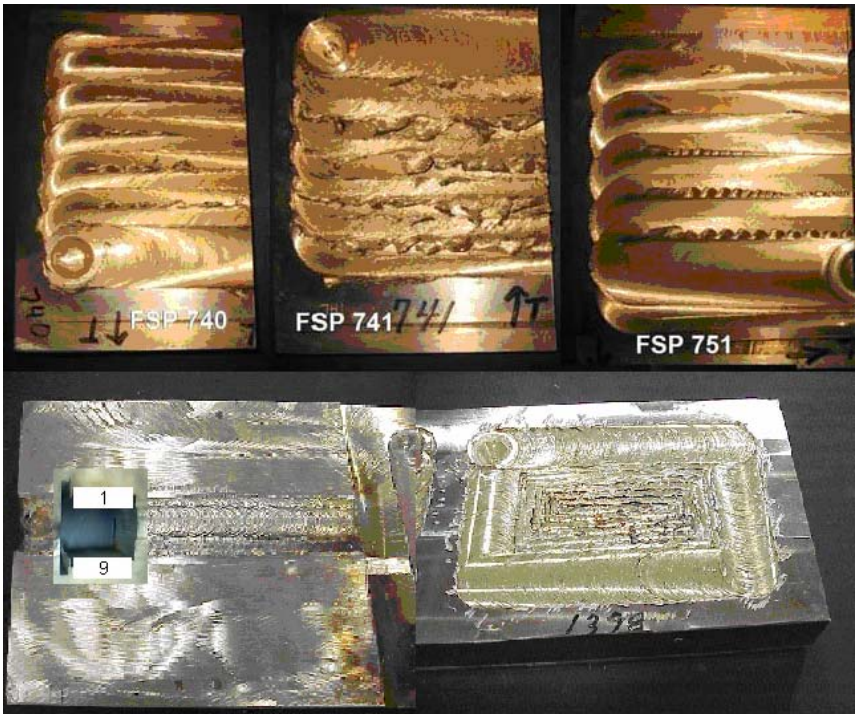

Figure 10. FSP and Fusion Weld NAB Material, with example of sectioning of miniature tensile specimen. The thickness of the fusion weld plate and 1398 FSP plate was 1.5 inches, while the 740, 741 and 751 FSP plates had a thickness of 0.3 inches.

Element	Cu	Al	Ni	Fe	Mn	Si	Pb
Min-Max	**(min)79.0**	**8.5-9.5**	**4.0-5.0**	**3.5-4.5**	**0.8-1.5**	**0.10(max)**	**0.03(max)**
Nominal	**81**	**9**	**5**	**4**	**1**	**-**	**-**
Alloy 1	**81**	**9.39**	**4.29**	**3.67**	**1.20**	**0.05**	**<0.005**
Alloy 2	**81.2**	**9.80**	**4.71**	**4.95**	**1.01**	**0.08**	**0.01**
740	**80.30**	**9.44**	**4.86**	**3.90**	**1.25**	**0.04**	**0.01**
741	**81.07**	**9.27**	**4.67**	**3.37**	**1.35**	**0.04**	**0.01**
751	**80.68**	**9.31**	**4.76**	**3.69**	**1.30**	**0.04**	**0.01**
Fusion Weld	**82.3**	**8.05-8.2**	**4.45**	**3.96**	**0.96**	**0.035**	**0.019**
1398	**80.6**	**9.54**	**4.96**	**3.71**	**0.96**	**0.27**	**-**

Table 1. Composition (wt%) of UNS C95800 NAB (After 21).

Coring and segregation effects may be responsible for the wide range of sample composition. Three of five samples did not meet the standards established in reference 17. Out-of-tolerance percentages are underlined. The material was processed using 6mm or 13mm stepped spiral tools. Table 2 summarizes the FSP parameters used for each run. For the fusion weld, 6 weld overlays went over a crack in NAB material. Moreover, the filler material used for the weld overlays was Amptrode 46, which has a composition similar to that of the fusion weld NAB plate. The thickness of the fusion weld plate and the 1398 plate was 1.5 inches, while the thickness of the plate of the 740, 741 and 751 FSP plate was approximately 0.3 inches.

FSP	Tool Size	Type	Pass/Pattern	RPM/IPM
740	6mm	Raster	Single/ Adv/Adv-Ret/Ret	Pass 1: 1000 / 4
741	6mm	Raster	Double/ Adv/Adv-Ret/Ret	Pass 1: 1000 / 4 Pass 2: 1000 / 4
751	6mm	Raster	Double/ Adv/Adv-Ret/Ret	Pass 1: 1000 / 4 Pass 2: 1000 / 10
1398	13mm	Spiral	Single/ Adv/Ret-Adv/Ret	Pass: 800/2

Table 2. FSP process histories (After 8).

C. MICROSCOPY

1. Sample Preparation

Sample sections from were prepared using the Charmilles Andrew EF630 electric discharge machine (EDM). Sections were mounted in 1.25 inch premold - red phenolic using a Buehler SIMPLIMET 2 mounting press. Mounted samples were mechanically polished following the schedule outlined in Table 3 for the indicated conditions using both Buehler ECOMET 4 and ECOMET 3 polishing wheels combined with the Buehler AUTOMET 2 powerhead. After polishing steps 4 – 7, the samples were ultrasonically cleaned in methanol for a minimum of 10 minutes. Samples were etched for 1 second in an etching solution of 40ml water, 40ml ammonium hydroxide and 2ml hydrogen peroxide and subsequently rinsed in water. They were then etched for 2 seconds in an etching solution of 60ml water, 30ml phosphoric acid and 10ml hydrogen peroxide and rinsed again.

Step	Abrasive	Time	RPM
1	400 Grit SiC Paper	30 sec.	90
2	1000 Grit SiC Paper	30 sec.	90
3	2400 Grit SiC Paper	30 sec.	90
4	4000 Grit SiC Paper	30 sec.	90
5	3 Micron Metadi Diamond Suspension	7 min.	150
6	1 Micron Metadi Diamond Suspension	7 min.	150
7	0.05 Micron Colloidal Silica	7 min.	40

Table 3. Mechanical Polishing Schedule.

2. Optical Microscopy

Optical microscopy was conducted using the Carl Zeiss JENAPHOT 2000, inverted reflected light photomicroscope, with output via a PULNIX TMC-74 – CCD Camera. The digital output was used with SEMICAPS photo capturing and measurement software.

THIS PAGE INTENTIONALLY LEFT BLANK

III. RESULTS AND DISCUSSION

Results of investigations into a fusion welded NAB as well as NAB materials processed by FSP will be presented in this chapter. The main focus is on the fusion-welded material and on FSP 751 and 1398 as representative examples of different processing approaches. Data for other conditions examined in the research are included in the Appendices.

A. STRENGTH AND DUCTILITY DISTRIBUTION OF FUSION WELD AND PRESENCE OF HIGH/LOW DUCTILITY REGIONS IN HEAT AFFECTED ZONE

All previous studies of FSP of NAB materials has suggested that low ductility in the vicinity of the SZ/TMAZ interface may be, at least in part, due to formation of low ductility martensitic transformation products of β produced by the process heat input. Similar features will be found in the HAZ of a fusion weld. For this reason, a fusion weld overlay was prepared in order to examine ductility distributions in this regard. Figure 11 shows a transverse section of the six weld passes that were placed in a groove machined in the surface of a NAB plate, as well as the indexing system for the location of tensile specimens machined from the plate. The vertical axis indicates the numbering of the sample with increasing depth. The centerline of the horizontal axis is indicated by the number “5.”

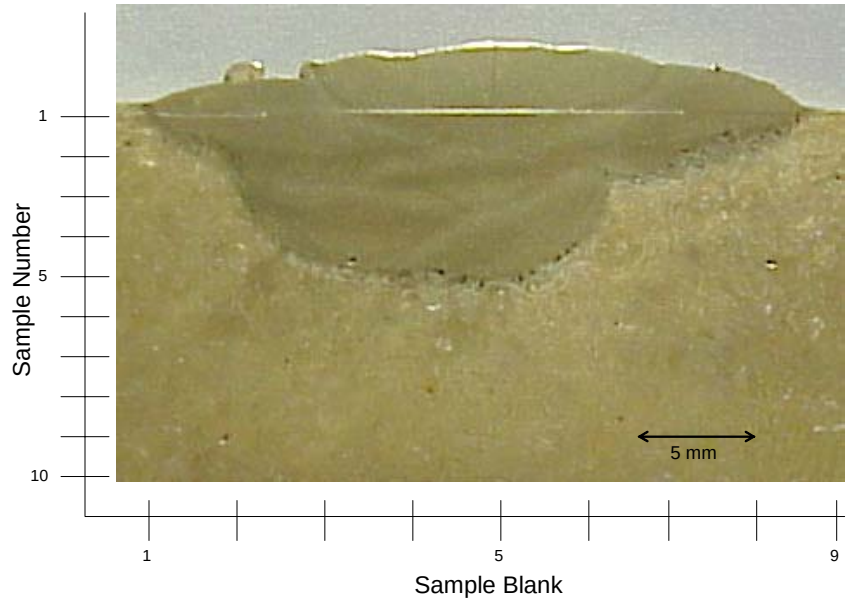

Figure 11. Schematic of Weld Pool, HAZ and Base Metal Illustrating Six Weld Passes and the Layout of the Locations of the Tensile Specimen Relative to Locations in the fusion weld. Highest ductilities were observed in the weld pool.

Figure 12 shows the stress strain data for the tests corresponding to the centerline of the fusion weld. At locations within the weld pool, the ductilities were in excess of 30 percent, and the tensile strengths are in excess of 700 MPa. The yield strengths were typically in the range of 200-290 MPa. However, at locations including the heat affected zone, the mechanical properties, and especially the ductility were drastically reduced. For example, at location 5 along both the vertical and horizontal in Figure 11, the ductility was approximately 3 percent. At locations where the tensile specimen was comprised of base metal, for example, at location 10 on the vertical axis at the centerline of the weld, the ductility was approximately 10 to 12 percent. This latter value conforms to ductility specifications for as-cast NAB materials [11].

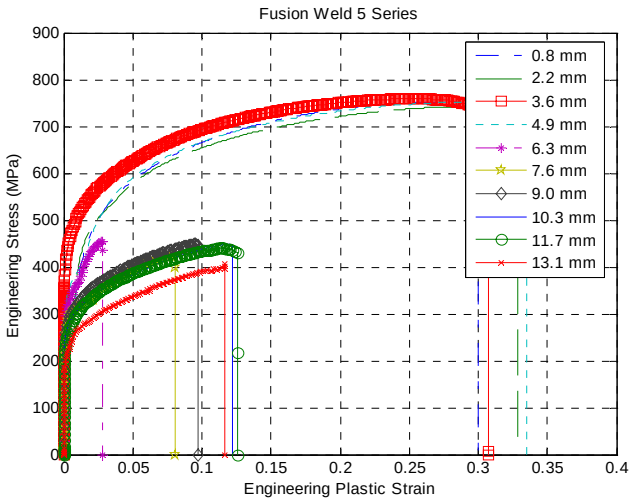

Figure 12. Stress-Strain Plot for Centerline of Fusion Weld. At locations in the weld pool, the ultimate strengths were in excess of 700 MPa, the yield strengths were in the range of 200-290 MPa. The ductilities were highest near the surface and lowest at locations associated with the heat affected zone.

The consolidation of mechanical property data for all of the tensile specimen for the fusion weld was conducted by using MATLAB to generate mesh plots. Figure 13 shows the ultimate yield strength, yield strength and plastic strain to failure as a function of position within and around the fusion weld. In this figure, the numbers 1, 5 and 9 on the distance axis correspond to blanks 1, 5 and 9 indicated in Figure 11. Figure 13a shows that the ultimate tensile strengths are ~ 700 MPa in the weld pool and drop to 400-450 MPa in base metal. Figure 13b shows that the highest yield strengths are in the weld pool, and are slightly lower in the rest of the material. Figure 13c illustrates high ductilities in the weld pool and a low ductility region (less than 10% elongation) in the HAZ surrounding the weld metal, followed by a subsequent increase in ductility on into the base metal.

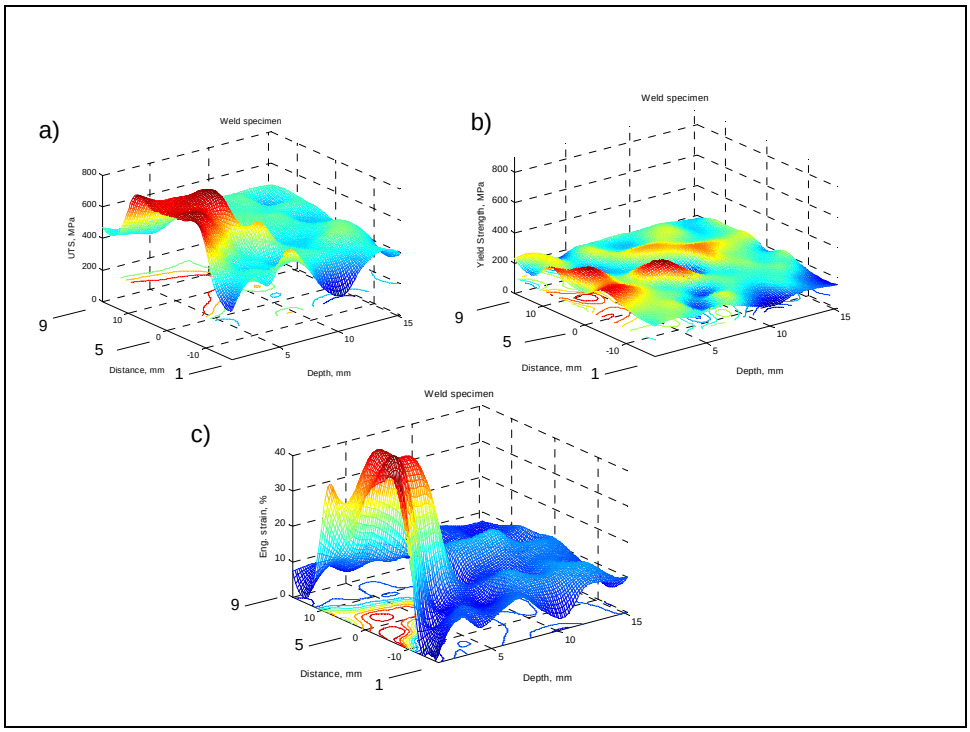

Figure 13. a) Ultimate Tensile Strength, b) Yield Strength and c) Ductility Distribution in a Fusion Weld as a function of depth and orientation. Ultimate Tensile Strengths and ductilities are highest in the weld pool

As shown in Figure 14a, the weld pool exhibited a Widmanstätten microstructure, similar to that associated with SZ locations after FSP. However, there were no coarse κ_{ii} particles due to the rapid rate of solidification. The Widmanstätten structure is consistent with relatively rapid cooling (rates ~ 10^0 °C/s) during welding when compared to propeller casting operations. Thus, the β formed upon solidification transforms partially to α with the Widmanstätten morphology and then, at lower temperatures to bainitic or martensitic products of β decomposition. These latter products are dark-etching and so delineate the Widmanstätten morphology of the α plane. As shown in Figure 14b, the fracture surface displayed microvoid formation and coalescence upon failure.

a) 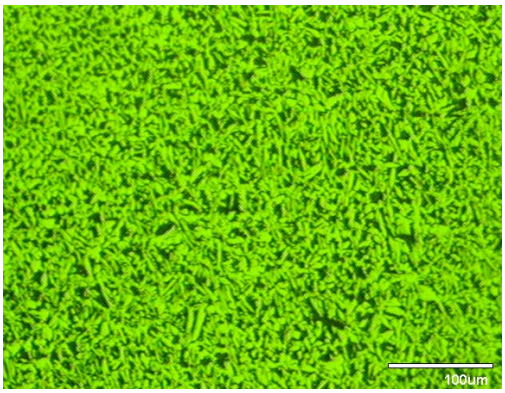

b) 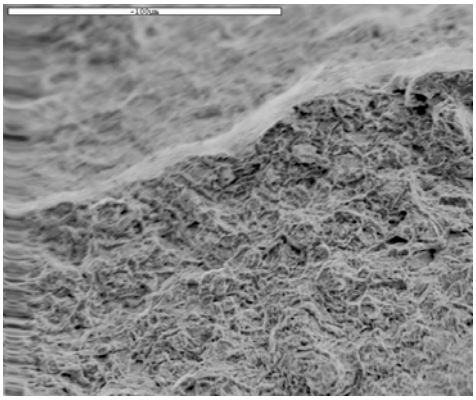

Figure 14. Widmanstätten Microstructure and Microvoid Formation and Coalescence in Fracture Surface of Weld Pool.

Figures 15a and 15b show the microstructure and fracture surfaces associated with material from locations in the HAZ, respectively. In the heat affected zone, the coarse $\alpha + \kappa_{iii}$ eutectoid constituent formed during the slow cooling following propeller casting will transform to β upon heating to T > 800°C. During subsequent rapid cooling, this β, which is higher in Al content, tends to transform to a martensite product. The appearance of this dark-etching product with untransformed primary α, indicates heating to 800-900°C; evidently, the martensite, or a mixture of it with the primary α, is brittle and this is reflected in the tensile data. It must also be noted that the mechanical property data suggest steep gradients in strength and ductility near the weld metal – HAZ interface. These gradients, if present within the gage section of a tensile sample, may, by themselves, result in low apparent ductility. A mixture of strong, ductile weld metal and soft, less ductile base metal would result in strain concentration in the softer regions and low apparent ductility. The fracture surface associated in the HAZ does not involve microvoid formation, and suggests that this material was heated into the eutectoid region.

a) 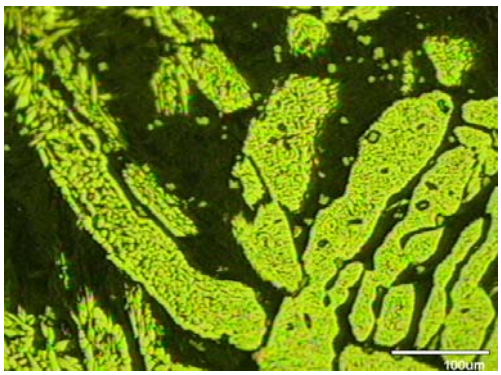 b) 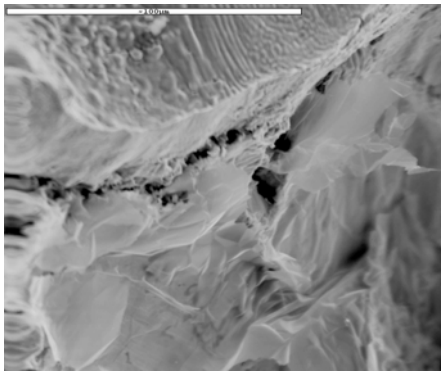

Figure 15. Microstructure and Fracture Surface of Heat Affected Zone in Fusion Weld. A composite type microstructure exists, primarily lamellar in nature. Microvoid formation is absent on the fracture surface.

Thus, the HAZ of a fusion zone is also a low ductility region in a fusion weld, in a similar manner to what has been previously observed in the TMAZ/HAZ boundary of a FSP material.

B. ISOTROPY OF STRENGTH AND DUCTILITY IN SINGLE-PASS AND MULTI-PASS RASTER FSP

A schematic illustrating the orientation of the tensile specimen axes, in both the longitudinal and the transverse senses, is shown in Figure 16.

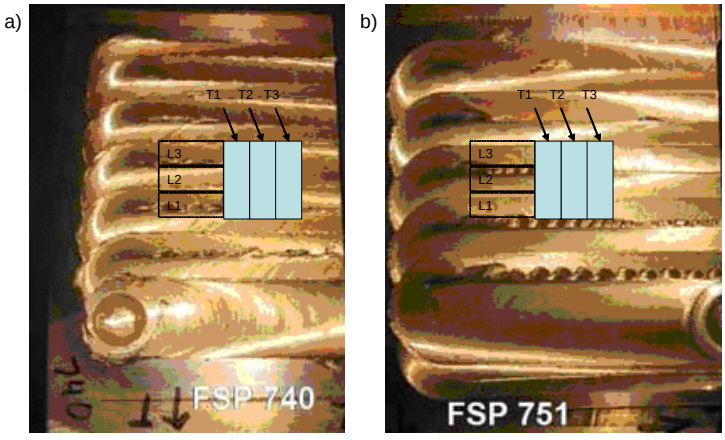

Figure 16. Schematic of 740 and 751 and Corresponding Orientations on Longitudinal (dashed rectangle) and Transverse (solid rectangle) Tensile Specimen.

1. Single-Pass Raster FSP

Mesh plots of tensile strength, yield strength and ductility were previously reported by Williams [8] and are included in Figure 17. These data were obtained for longitudinal tensile axis orientations. Samples having a transverse orientation, as indicated in Figure 16, will exhibit property variation only with depth.

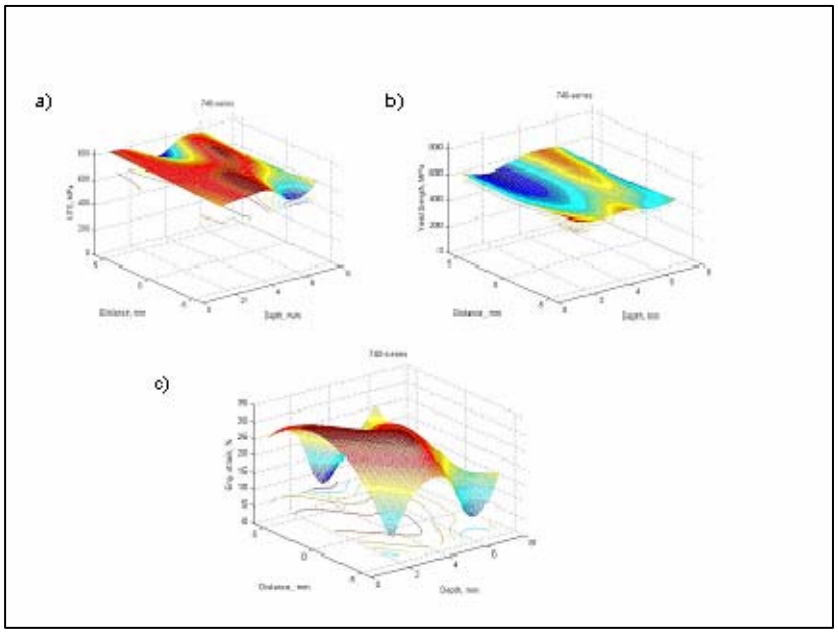

Figure 17. 3-D Representation of Strength and Ductility Distribution as a Function of Depth and Orientation for Single-Pass Raster FSP (After 8). Mechanical properties along the centerline will be compared to averaged properties in a transverse orientation.

Thus, to provide a comparison between longitudinal and transverse properties in FSP of NAB, the centerline results, ie, at a distance of 0 mm in Figure 17 obtained by Williams, were compared to the averaged properties in the transverse direction of the same material. Transverse samples were sectioned such that the samples resided in the stir zone. A two dimensional representation of mechanical properties as a function of depth were constructed and are shown in Figures 18-20.

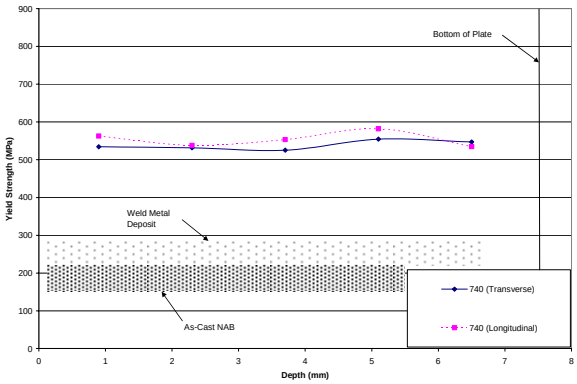

Figure 18. Yield Strength Distribution as a Function of Depth in 740 FSP Material.

As shown in Figure 18, the yield strengths were essentially isotropic and were larger than yield strengths in a fusion weld by a factor of two or more, 500+ MPa in the SZ as opposed to 200+ MPa in weld metal. Also, the ultimate strengths were isotropic in the SZ, and were 700-800 MPa, as shown in Figure 19.

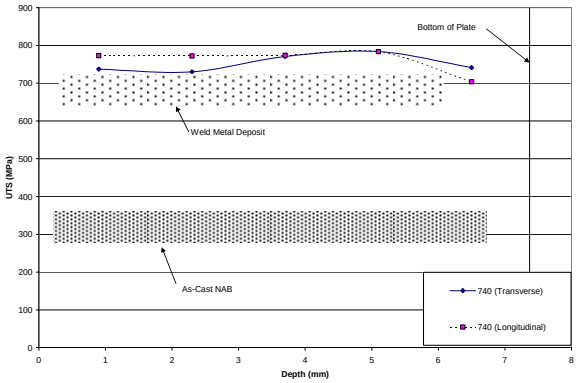

Figure 19. Ultimate Tensile Strength Distribution as a Function of Depth in Single Pass FSP.

However, ductility was not isotropic. The plastic strains in single-pass raster FSP were higher in a longitudinal sense when compared to a transverse orientation, as displayed in Figure 20. This result may be attributed to several factors. These include the possibility that gage sections may have a combination of advance-advance and retreat-retreat regions, as suggested in Figure 3. Here, a reduction of mechanical properties is expected in that the retreat/retreat microstructures may have experienced

less overall strain than advance/advance regions. Thus, transverse samples may have property variations along the tensile axis. Also, tool wear, as well as surface roughness, may have played a factor in this result. Indeed, ductility differences are greatest at the plate surface and so removal of a layer of material may ensure isotropy of all mechanical properties.

The thickness of the FSP 740 plate is approximately 7.5 mm and this did not allow determination of the reduction of properties associated with the transition through the TMAZ and base metal in this case. The location of the bottom of the plate is indicated in Figures 18-20.

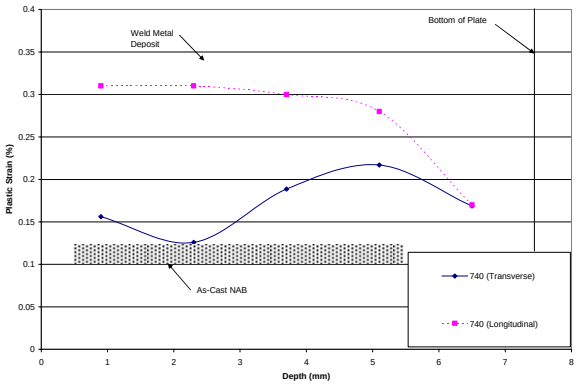

Figure 20. Ductility Distribution as a Function of Depth in Single Pass FSP.

2. Multi-Pass Raster FSP

Mesh plots were previously developed by Williams [8] and are shown in Figure 21. Again, the centerline results, i.e., at a distance of 0 mm in Figure 21, were compared to the averaged properties in the transverse direction of this material. Again, transverse samples were sectioned such that the samples primarily resided in the stir zone.

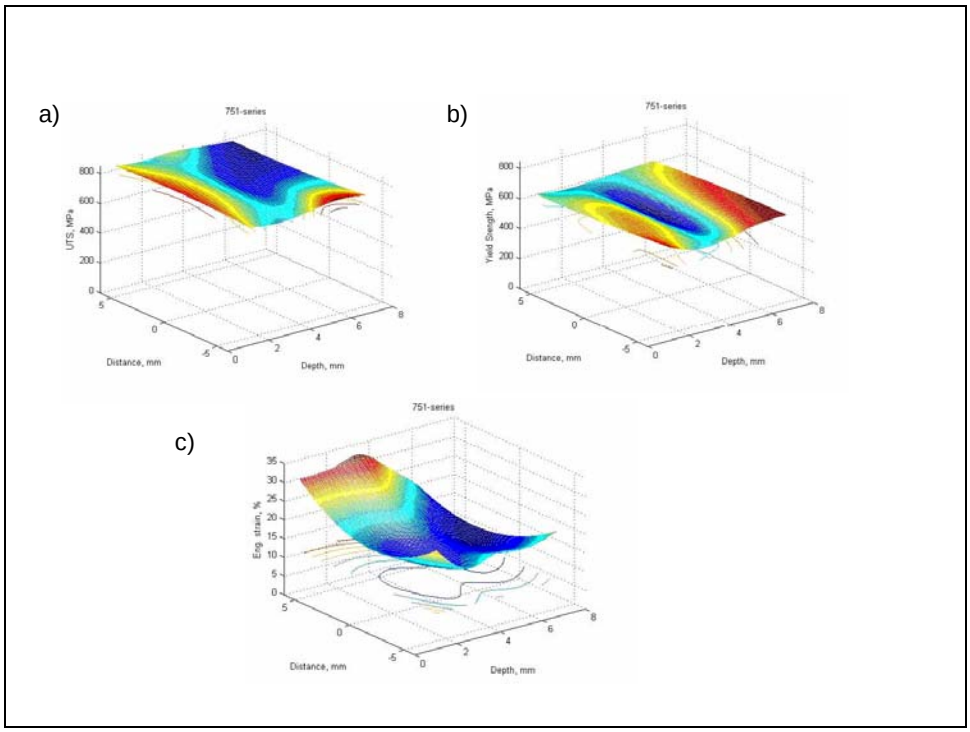

Figure 21. 3-D Representation of Strength Distribution as a Function of Depth in 751 Multi Pass FSP (From 8).

Two dimensional representations of mechanical properties as a function of depth were constructed and are shown in Figures 22-24.

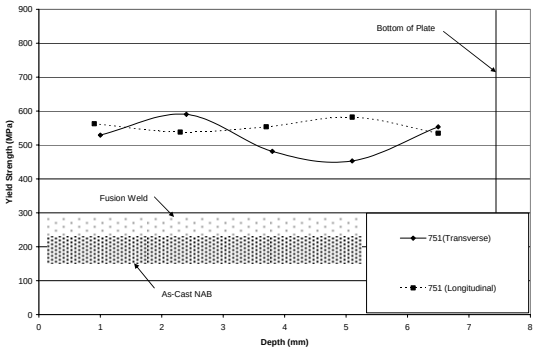

Figure 22. Yield Strength Distribution as a Function of Depth in 751 Series.

As shown in Figures 22 and 23, the yield strengths and ultimate tensile strengths were isotropic, as long as the material resided in the stir zone.

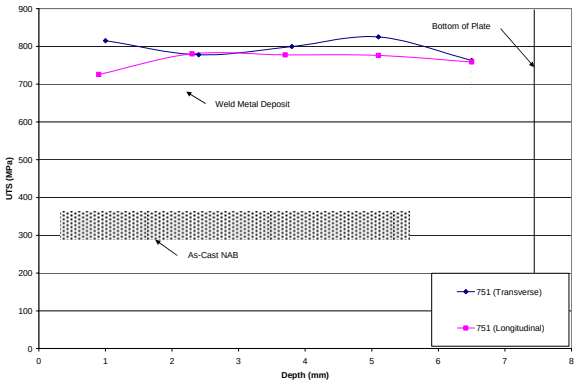

Figure 23. Ultimate Tensile Strength Distribution as a Function of Depth in 751 Series.

In mutli-pass FSP material using a raster pattern, the ductilities were significantly larger in a transverse orientation when compared to the longitudinal orientation, as shown in Figure 24. The transverse samples were taken within the SZ. In multi-pass processes, it is likely that gradients along the transverse direction may be reduced and this may account for improved ductility. However, similar, high ductility would be expected in longitudinal samples. This requires further investigation.

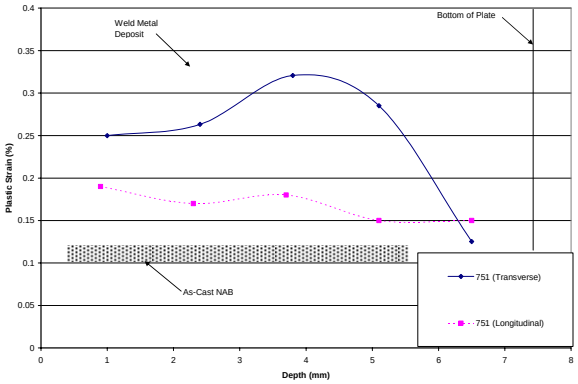

Figure 24. Ductility Distribution as a Function of Depth in Multi-Pass FSP.

When testing the single-pass and multi-pass raster material, the gage length was 7.7 mm, while the spacing between passes was approximately 3.5 mm. Thus, a minimum of two interfaces existed in multi-pass material in both cases. Figure 25 illustrates the homogeneity and the continuity of interfaces within the SZ. An optical microscopy examination of the interface region in a single linear pass (sample 858) is shown in Figure 25c and illustrates failure of the SZ-TMAZ interface during longitudinal testing of a sample having a composite microstructure.

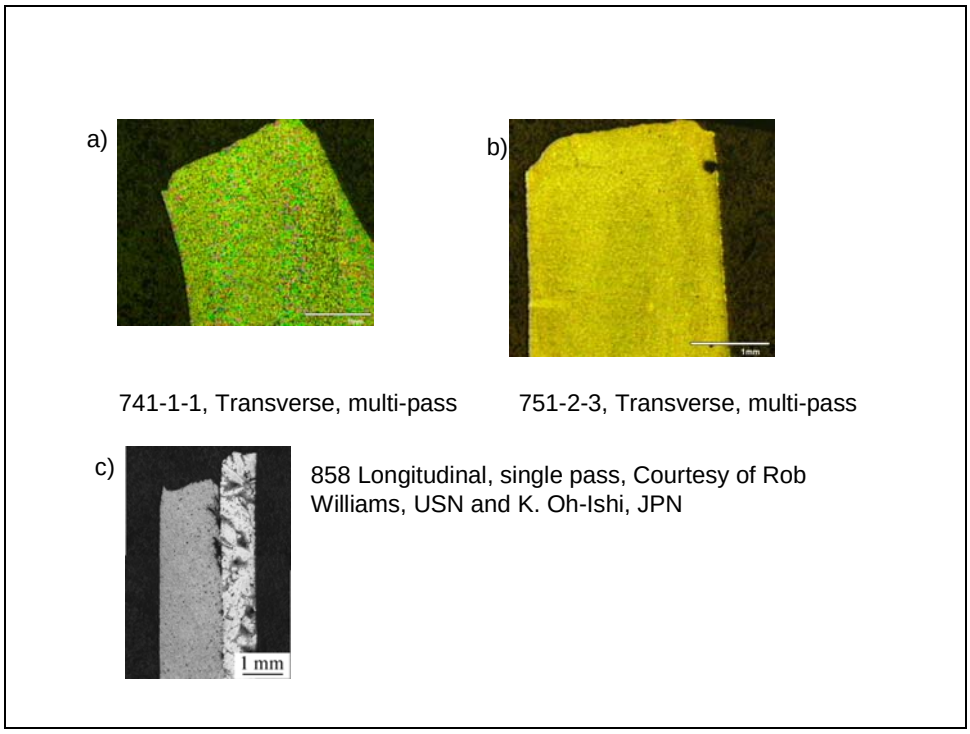

Figure 25. Testing of Successive Passes in Multi Pass FSP and Breakdown of Interface in Single Pass FSP. The interfaces within the SZ did not contribute to the reduction of mechanical properties.

Figure 25c suggests that solid state bonding between the microstructure associated with the TMAZ and the SZ may sometimes be unsound.

Figure 26 illustrates that the microstructure and fracture surfaces of both fusion welds and multi-pass raster FSP material are very similar in the weld pool and SZ, respectively.

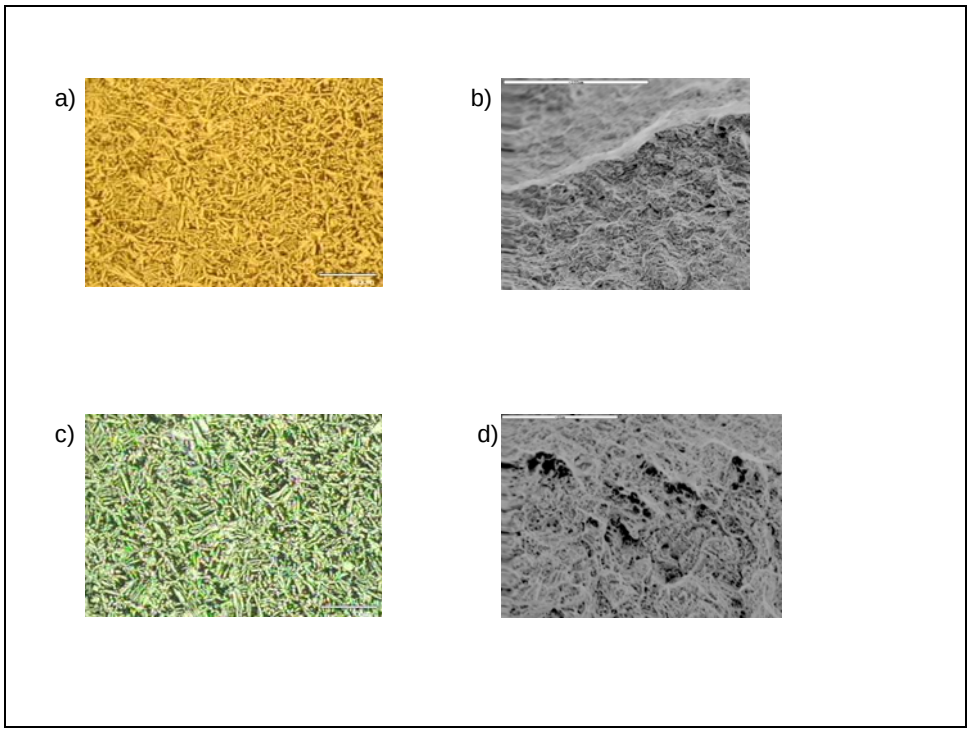

Figure 26. Widmanstätten Microstructures in Both Weld Metal, indicated in a) and Stir Zone, indicated in c) in FSP 751 material. Microvoid formation and coalescence were apparent in both weld metal (b) and the stir zone in FSP 751 material

Moreover, the fracture surfaces were similar, since both exhibited evidence of microvoid formation and coalescence. Both microstructures are Widmanstätten, while κ_{ii} particles were present in the SZ of FSP material, as shown in Figure 26c, which provide evidence of a slower rate of cooling relative to the solidification of the weld. The high yield strength of the FSP material must reflect a contribution of strain hardening despite the high deformation temperatures experienced by this material.

C. STRENGTH AND DUCTILITY DISTRIBUTION IN FSP NAB USING A SPIRAL PATTERN; HIGH/LOW DUCTILITY REGIONS.

1. Strength and Ductility Distributions

A spiral pattern was used in friction stir processing and its associated mechanical properties were observed in both longitudinal and transverse orientations. All tensile specimen were sectioned so that the gage length was comprised of material having multiple passes within the single spiral pattern. Widmanstätten microstructures observed in single-pass and multi-pass raster FSP material were not apparent. Instead, the stir zone consisted mainly of fine, equiaxed, α grains and dark-etching transformation products of β, as shown in Figure 27.

a) 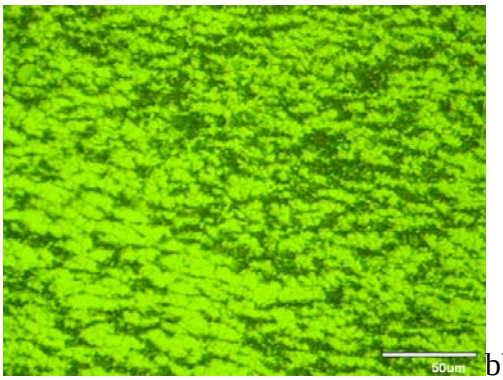 b) 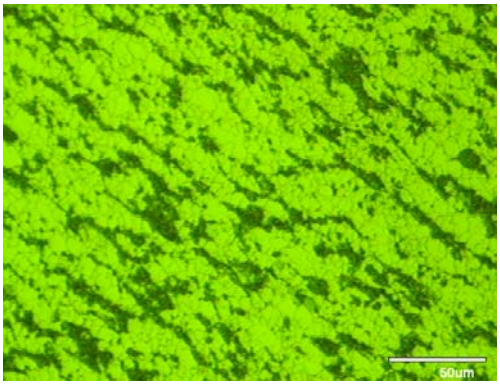

Figure 27. Fine Alpha Grains in Spiral Pattern at (a) the top of the stir zone and (b) the middle of the stir zone. Ductilities in the aforementioned regimes were in excess of 20 percent.

Figure 28 shows stress-strain curves for the spiral pattern material. At locations near the surface, the ductilities were in excess of 20 percent, with a reduction of ductility at increasing depths, associated with the transition through the TMAZ as well as porosity within base metal. This is particularly apparent in the fracture surface of a sample that exhibited 2 % elongation, which was located at a depth of 12.3 mm.

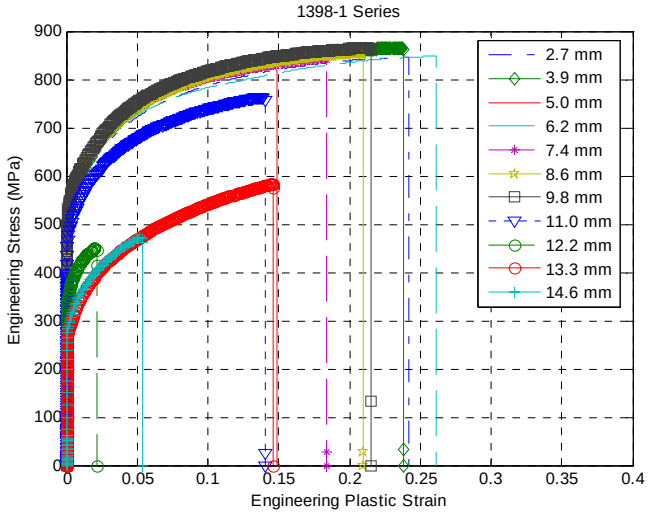

Figure 28. Stress-Strain Plot of 1398 Series in Longitudinal Direction.

Corresponding mesh plots for the longitudinal data are shown in Figure 29.

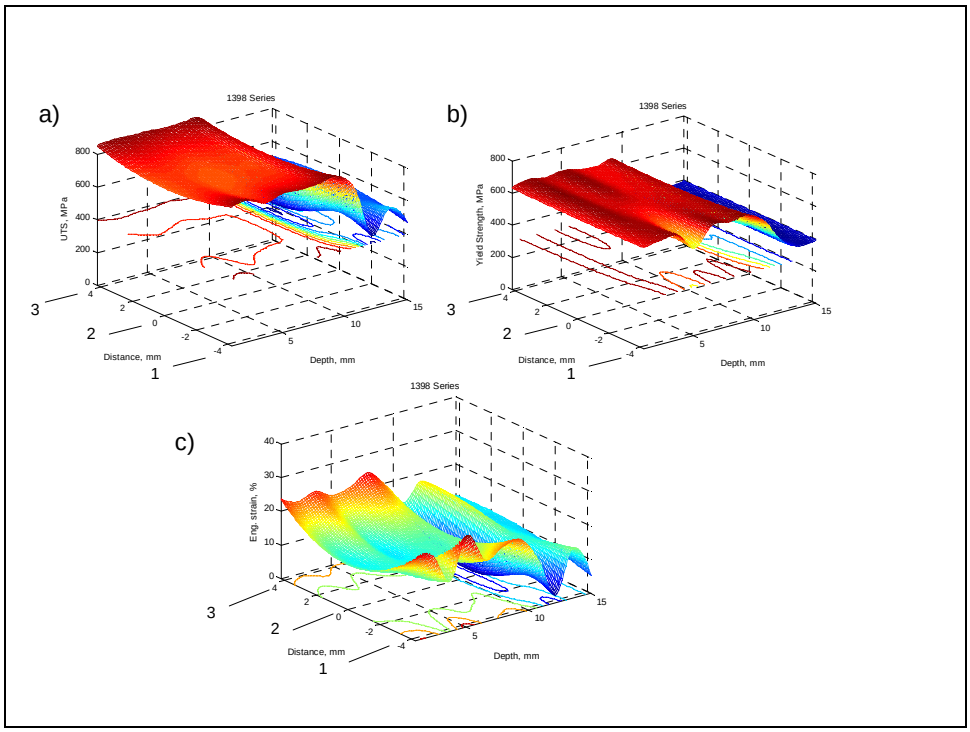

Figure 29. Strength and Ductility Distribution in 1398 Series

As shown in Figure 29, the yield and ultimate strengths were uniform across several adjacent passes. The ducilities, however, showed decreases with increasing depths associated with the TMAZ and subsequent changes in ductilities associated with the amount of porosity in base metal.

An average of the three blanks as a function of depth in the longitudinal directions was compared to the average of two transverse blanks in a similar fashion to test for isotropy of mechanical properties in a spiral pattern along various planes in this material. Figures 30, 31 and 32 are comparative plots of mechanical properties as a function of depth.

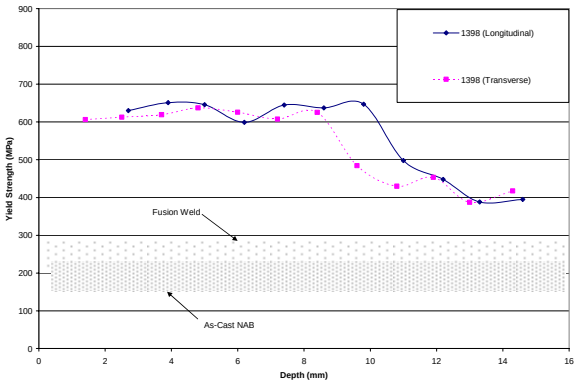

Figure 30. Yield Strength Distribution as a Function of Depth in 1398 Series.

Figure 30 illustrates that that the yield strengths are at least twice as large in the spiral pattern when compared to fusion weld data. Also, the yield strength data are nearly isotropic. As shown in Figure 31, the ultimate tensile strengths were also isotropic with increasing depth, and > 800 MPa in the stir zone.

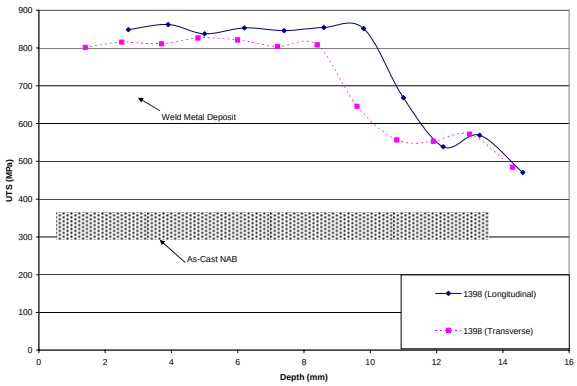

Figure 31. Ultimate Strength Distribution as a Function of Depth in 1398 Series.

Figure 32 illustrates that the ductility associated with a spiral pattern is more nearly isotropic as a function of depth. The ductilities are again largest in the SZ and initially decrease in the vicinity of the SZ/TMAZ interface. Low base metal ductility was often associated with porosity; it should be noted that the small gage cross section will result in a greater adverse effect of porosity on ductility than a larger gage cross section.

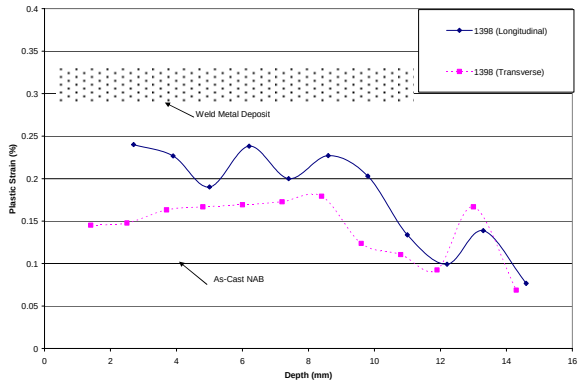

Figure 32. Ductility Distribution as a Function of Depth in 1398 Series.

2. Microstructure

Figure 33 shows the equiaxed, α grains in the SZ of the spiral pattern, at a depth of 6 mm, where the ductility was 27 percent. Moreover, the presence of microvoids is apparent in the fracture surface, as shown in Figure 33b.

a) 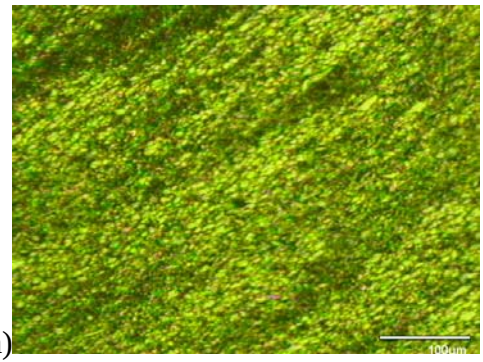 b) 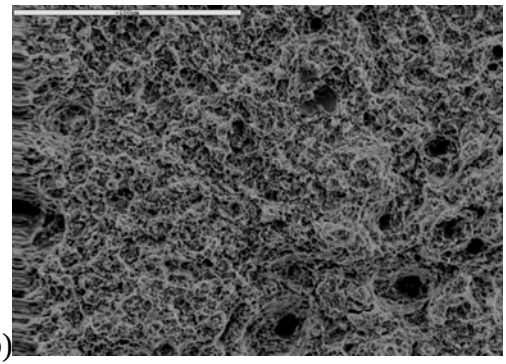

Figure 33. Microstructure (a) and Fracture Surface (b) of SZ of 1398 Series. The microstructure consisted of fine α grains and microvoids were observed in the fracture surface, resulting in higher levels of ductility.

Figure 34 shows the microstructure and fracture surface of base metal along with the evidence of porosity, where the elongation was approximately 2 percent.

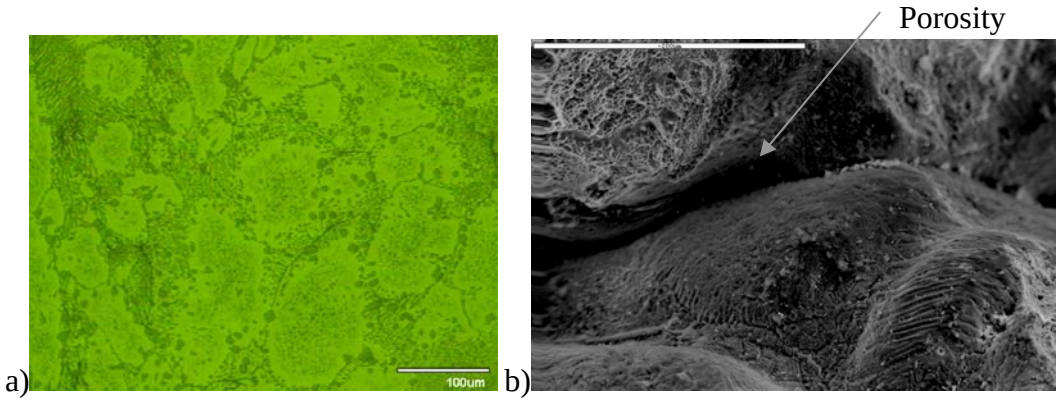

a) b)

Figure 34. Microstructure (a) and Fracture Surface (b) of Base Metal With Porosity. Ductilities were less than two percent. The microstructure of the base metal contains α grains, as well as κ_{ii} and κ_{iii} particles.

Low regions of ductility in the spiral pattern were associated with the mixture of microstructures, in the vicinity of the TMAZ. It appears that the spiral pattern leads to a reduction of ductility at regions near the TMAZ, but to a lesser extent than raster patterns or in fusion welds. However, there were locations where the ductility was below 10 percent in the TMAZ of a spiral pattern as well. Montages of both the spiral pattern and fusion weld material were created at 48X magnification. Figure 35 shows a comparison of the regions of low ductility in both the spiral pattern and fusion welds. The HAZ in conventional welds and the TMAZ in FSP material are both apparently culprits for reduced ductility and elongation values lower than as-cast material (approximately 10 percent). This suggests that ductility criteria for FSP not be more stringent than for fusion welds.

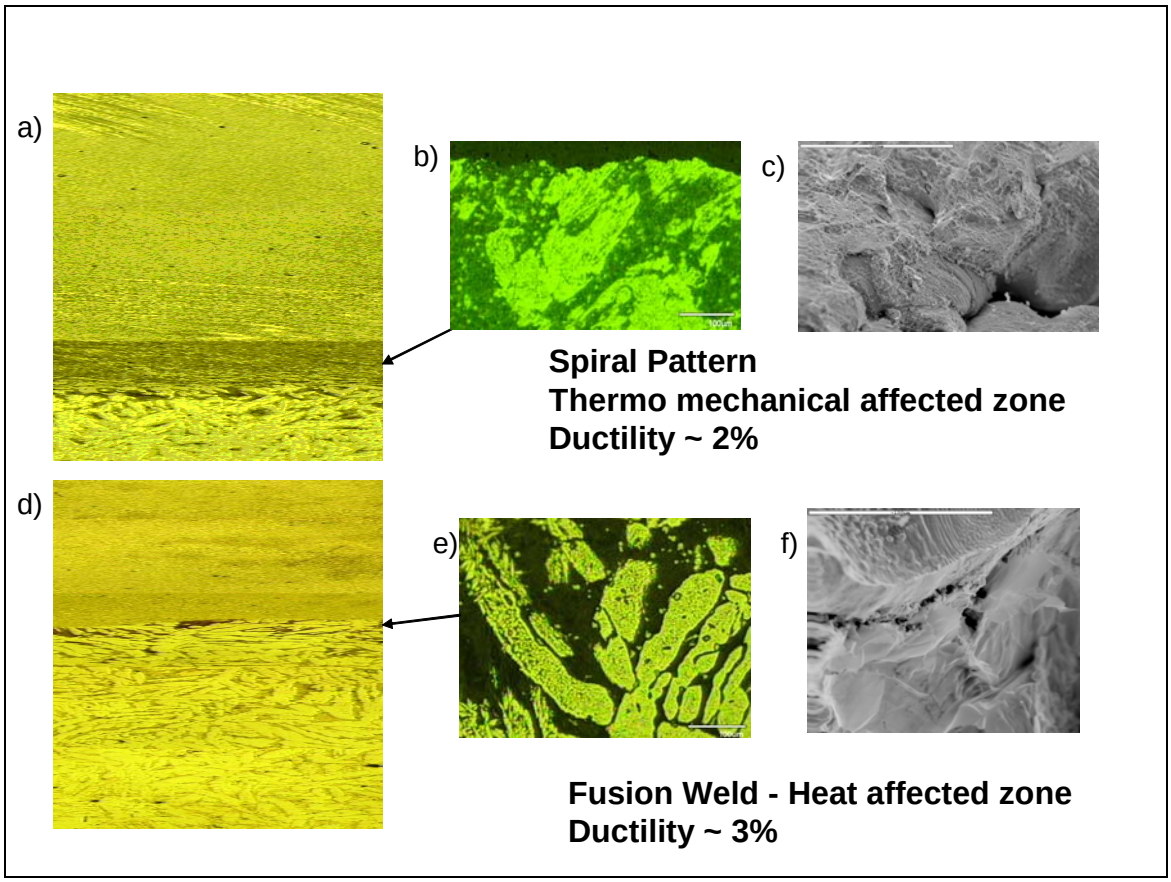

Figure 35. Regions of Lower Ductility in Fusion Weld and FSP NAB (Spiral Pattern). (a) and (d) are montages of the spiral pattern and fusion weld, respectively. Crack growth is preferred where there was the dark etching martensite, shown in (b) and (e). Also, the fracture surfaces exhibited some porosity and rock-candy surfaces, shown in (c) and (f).

THIS PAGE INTENTIONALLY LEFT BLANK

IV. CONCLUSIONS AND RECOMMENDATIONS

A. CONCLUSIONS

1. Fusion Weld NAB

a. The ultimate tensile strengths in Fusion Weld (FW) NAB were comparable to FSP NAB, but the yield strengths were only slightly higher than base metal and less than FSP NAB by at least a factor of two.

b. Areas of high ductility in FW material were due to the Widmanstätten microstructure and were similar to microstructures observed in multi-pass FSP NAB.

c. Areas of low ductility were evident in FW material, where a boundary including the heat affected zone was located.

2. Single and Multi Raster FSP NAB

a. In single-pass and multi-pass raster FSP NAB, the ultimate and yield strengths were isotropic.

b. The ductilities in raster NAB were anisotropic. Moreover, the ductilities were greater in the longitudinal orientation in comparison to the transverse orientation in single pass raster NAB. For multi-pass raster FSP NAB, the ductilities were greater in the transverse direction relative to the longitudinal orientation.

3. Spiral Pattern FSP NAB

a. The spiral pattern provided isotropy of all mechanical properties, including the ductility.

b. Areas of high ductility were due to the presence of fine α grains.

c. Areas of low ductility were due to the presence of TMAZ in a composite type microstructure. Therefore, the HAZ in conventional welds and the TMAZ in FSP material both exhibited regions of low ductility Thus, stricter design criterion cannot be placed on FSP material relative to conventional welds.

B. RECOMMENDATIONS FOR FUTURE RESEARCH

The following areas are recommended for future research:

1. Examine transverse interfaces where there is a possibility of mixed microstructures.

2. Compare microstructures and mechanical properties of FW/FSP process and FSP for future applications.

3. Expand RPM/IPM ranges to facilitate the prediction of microstructure and mechanical properties of FSP and further examine the question of mixed microstructures.

4. Conduct mechanical testing of fusion weld material in a transverse orientation.

APPENDIX A - STRESS VS. STRAIN PLOTS

A. 740 SERIES (TRANSVERSE)

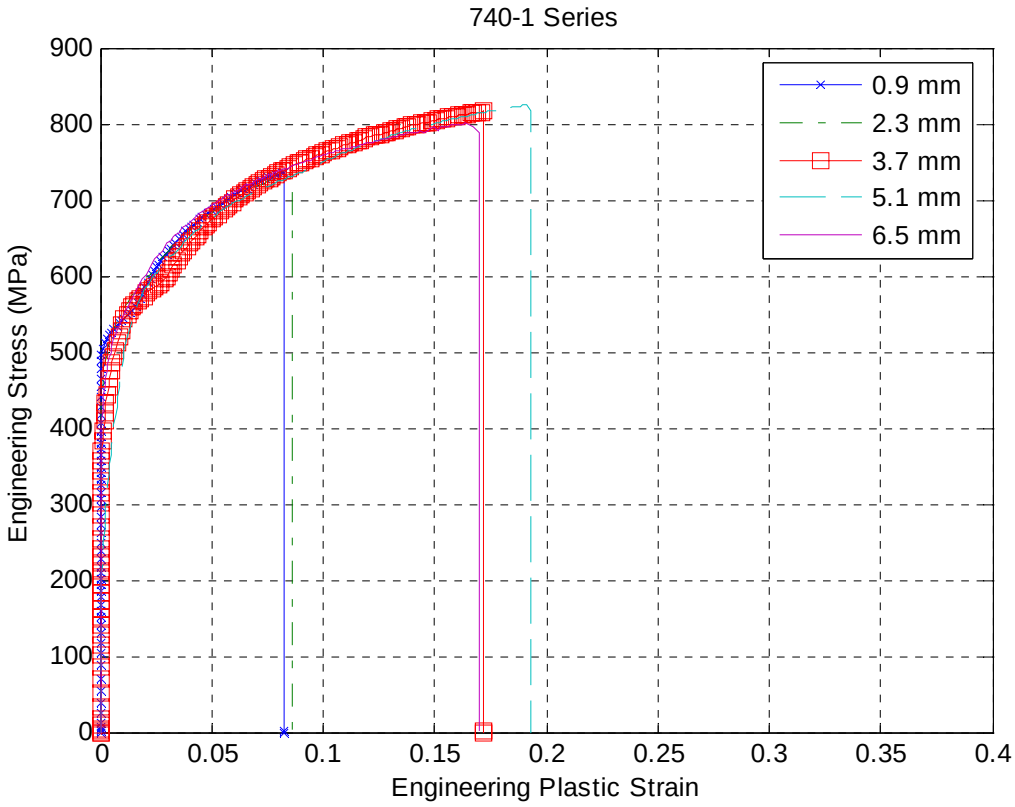

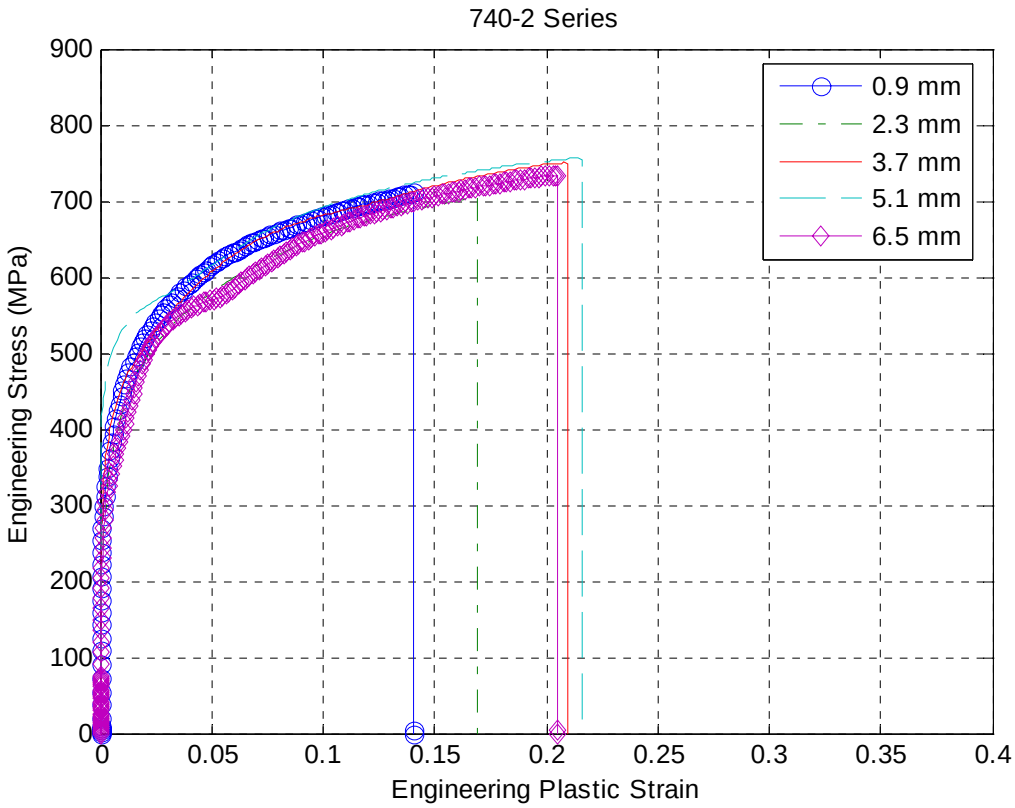
740-2 Series
Engineering Stress (MPa)
Engineering Plastic Strain
0.9 mm
2.3 mm
3.7 mm
5.1 mm
6.5 mm
0
100
200
300
400
500
600
700
800
900
0
0.05
0.1
0.15
0.2
0.25
0.3
0.35
0.4

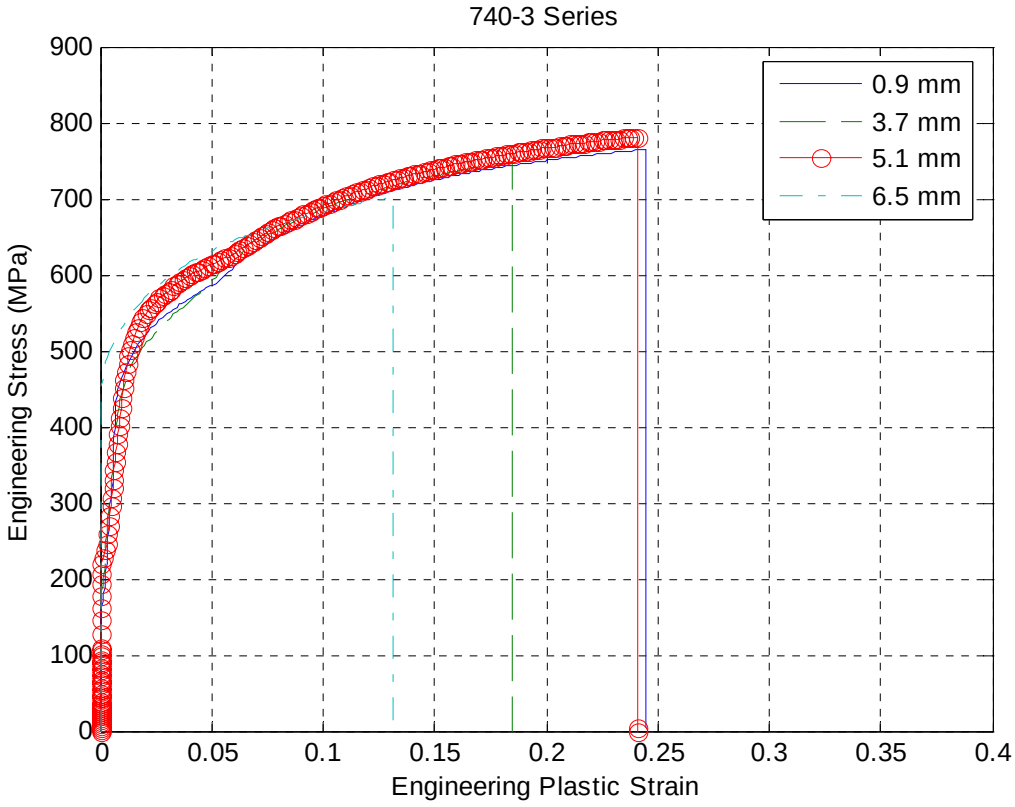
740-3 Series
Engineering Stress (MPa)
Engineering Plastic Strain
0.9 mm
3.7 mm
5.1 mm
6.5 mm
0
100
200
300
400
500
600
700
800
900
0
0.05
0.1
0.15
0.2
0.25
0.3
0.35
0.4

B. 741 SERIES (TRANSVERSE)

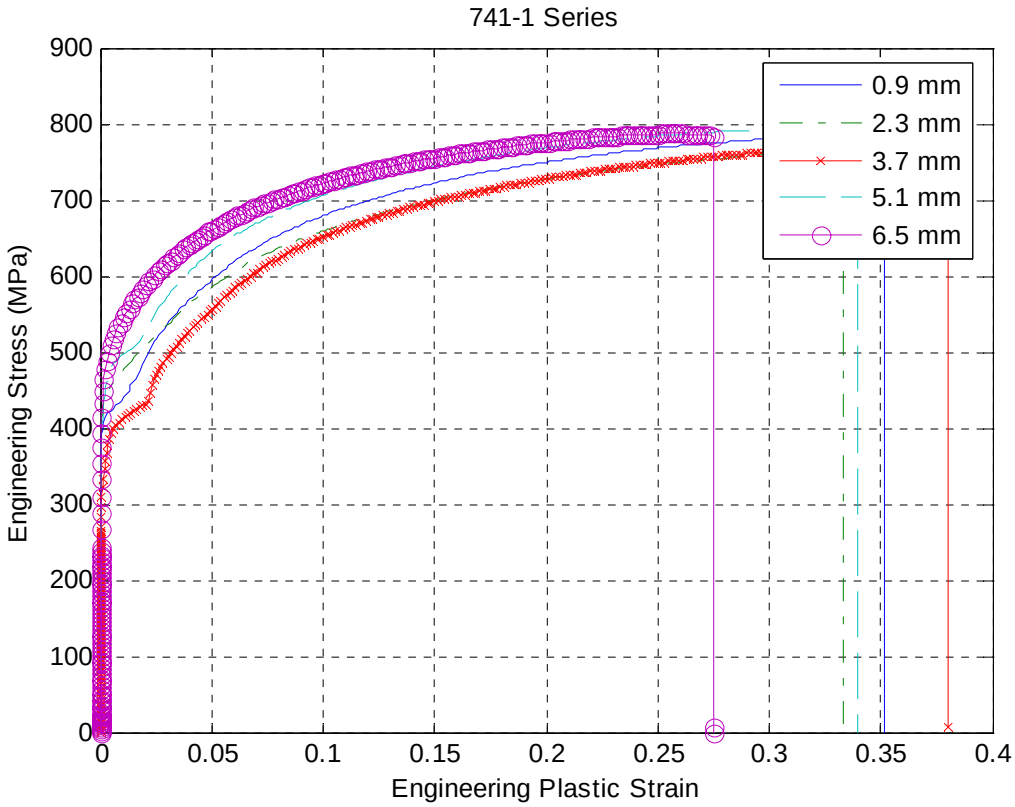

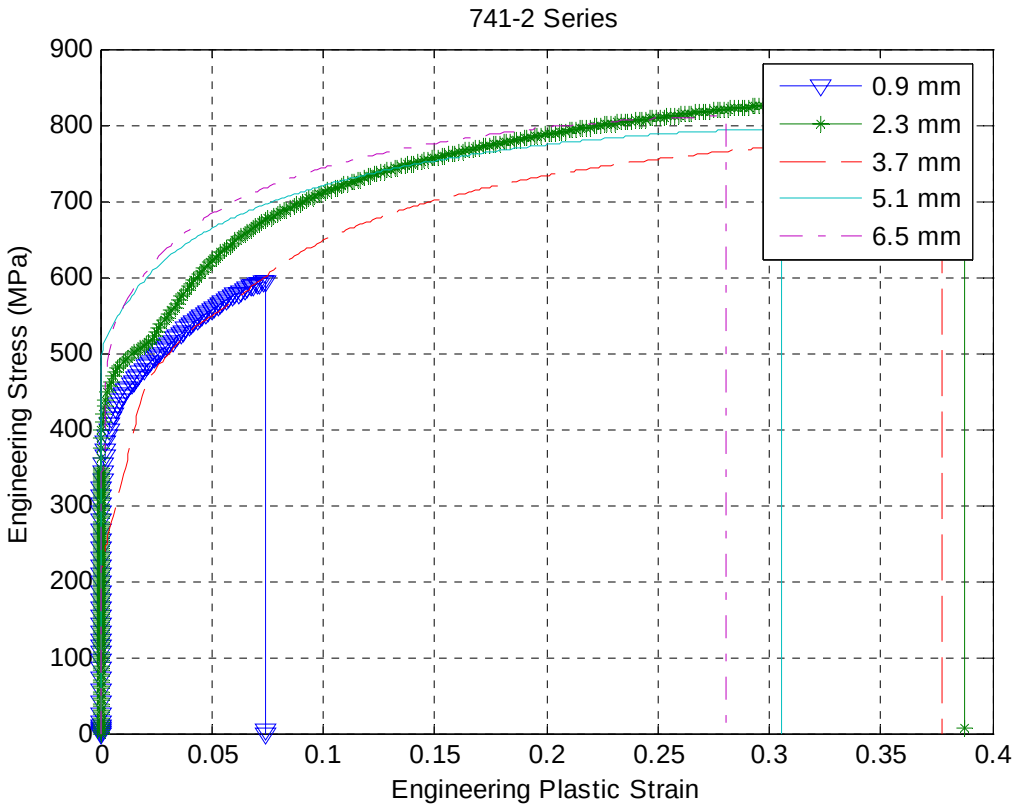
741-2 Series
Engineering Stress (MPa)
Engineering Plastic Strain
0.9 mm
2.3 mm
3.7 mm
5.1 mm
6.5 mm
0
100
200
300
400
500
600
700
800
900
0
0.05
0.1
0.15
0.2
0.25
0.3
0.35
0.4

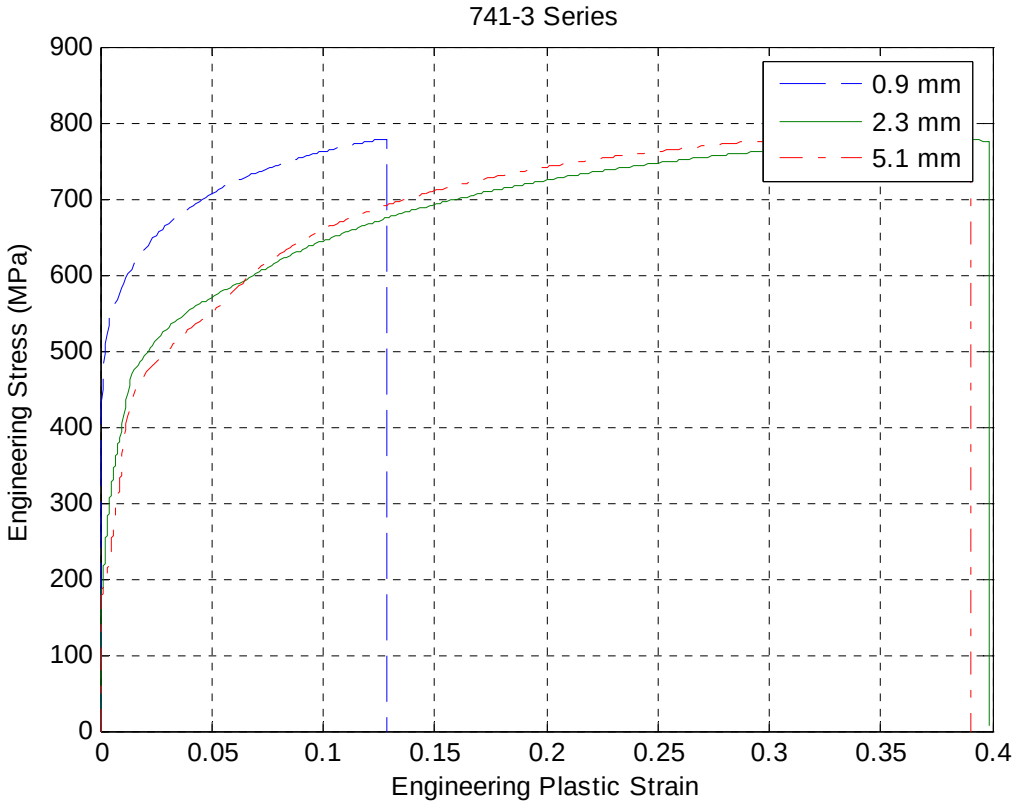
741-3 Series
Engineering Stress (MPa)
Engineering Plastic Strain
0.9 mm
2.3 mm
5.1 mm
0
100
200
300
400
500
600
700
800
900
0
0.05
0.1
0.15
0.2
0.25
0.3
0.35
0.4

C. 751 SERIES (TRANSVERSE)

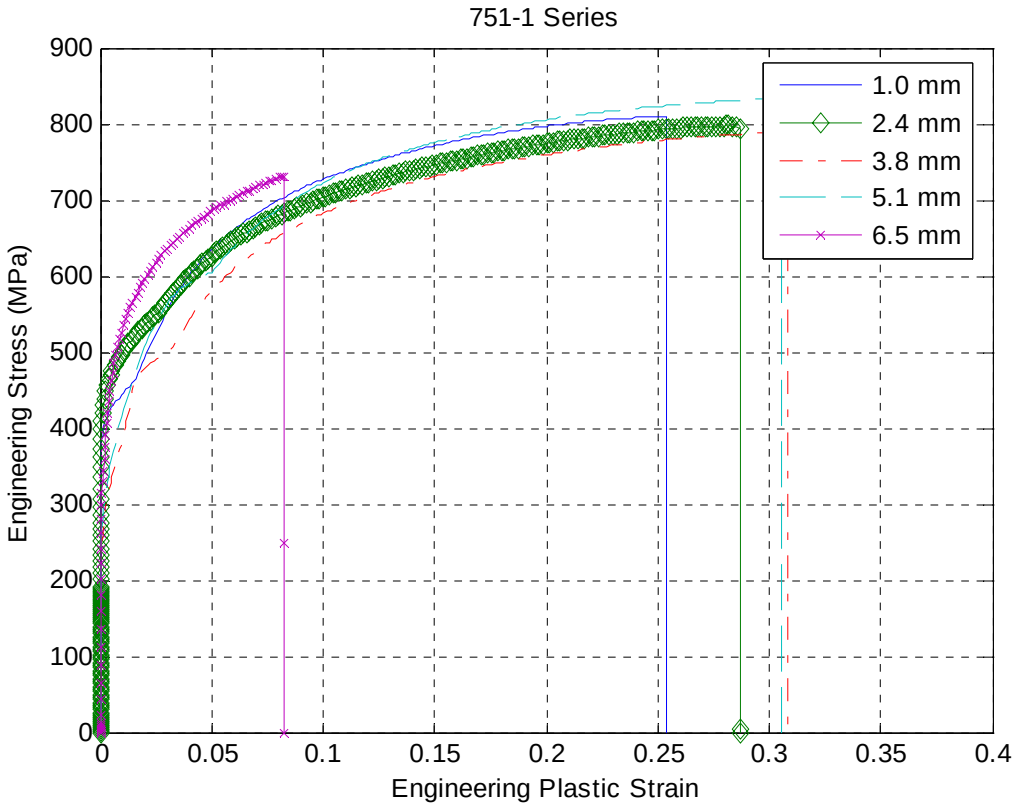

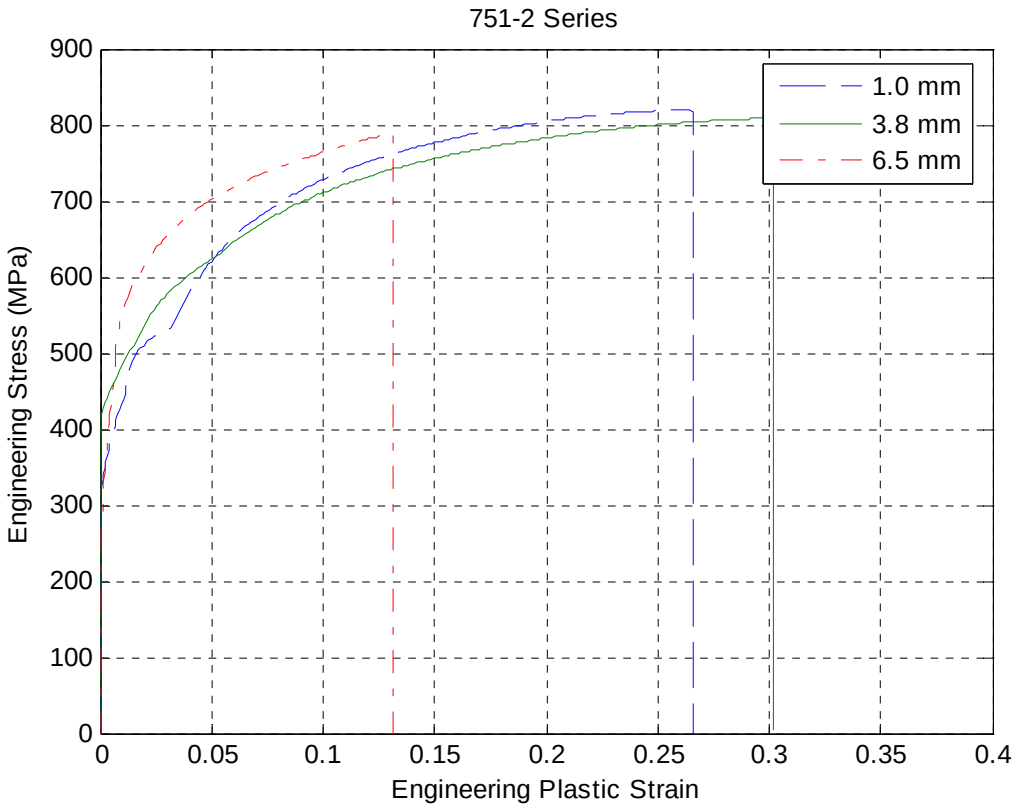
751-2 Series
1.0 mm
3.8 mm
6.5 mm
Engineering Stress (MPa)
Engineering Plastic Strain
0
100
200
300
400
500
600
700
800
900
0
0.05
0.1
0.15
0.2
0.25
0.3
0.35
0.4

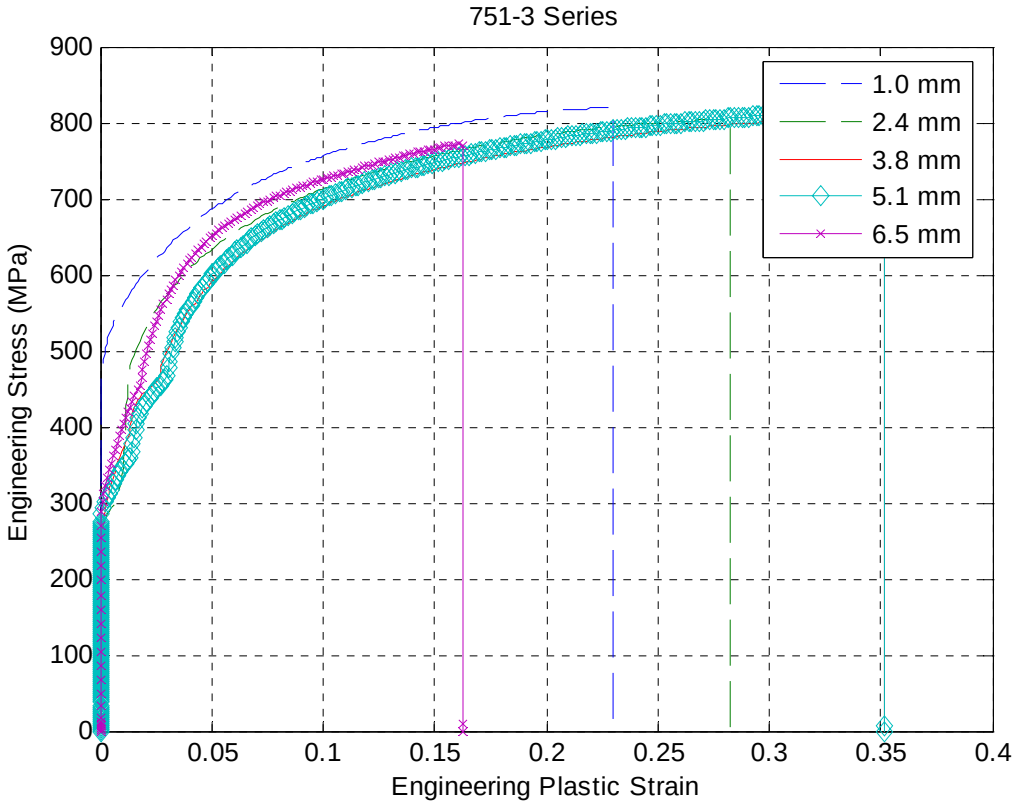
751-3 Series
1.0 mm
2.4 mm
3.8 mm
5.1 mm
6.5 mm
Engineering Stress (MPa)
Engineering Plastic Strain
0
100
200
300
400
500
600
700
800
900
0
0.05
0.1
0.15
0.2
0.25
0.3
0.35
0.4

D. FUSION WELD (LONGITUDINAL)

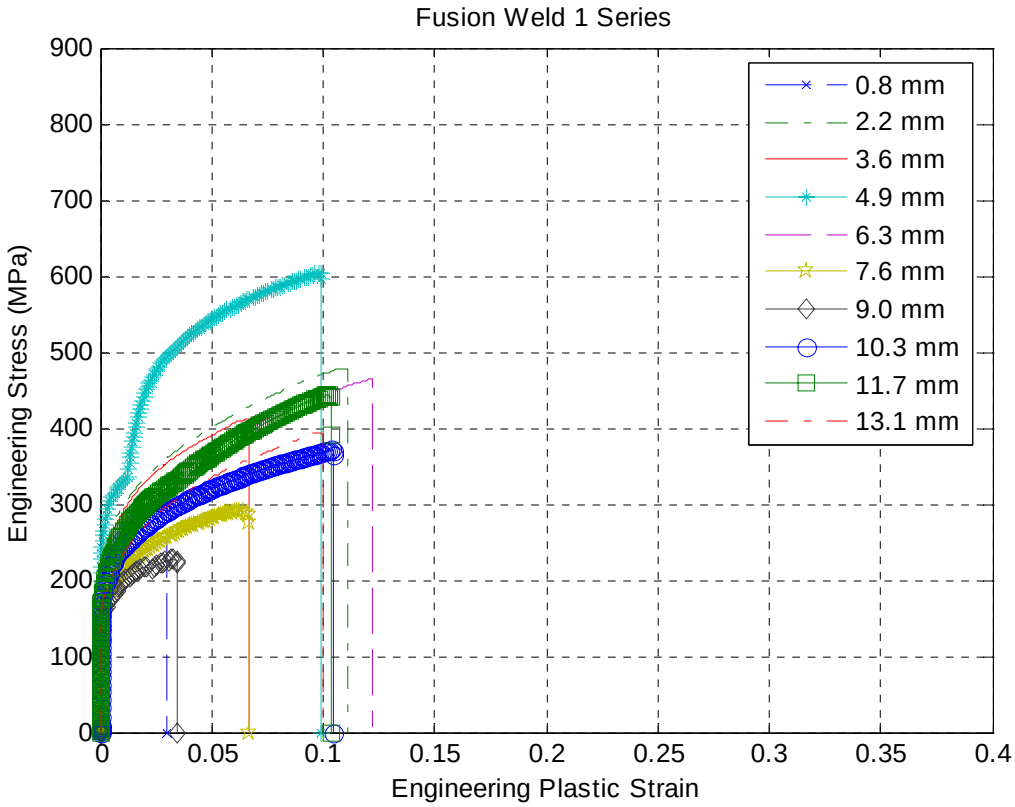

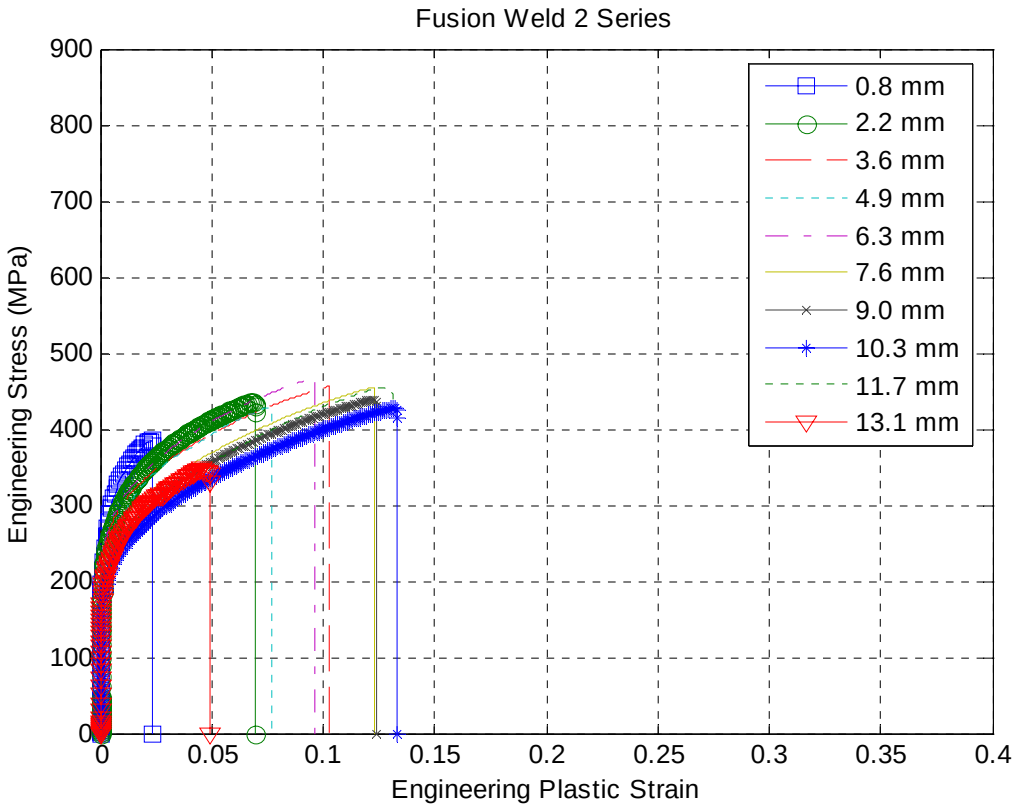
Fusion Weld 2 Series
Engineering Stress (MPa)
Engineering Plastic Strain
0.8 mm
2.2 mm
3.6 mm
4.9 mm
6.3 mm
7.6 mm
9.0 mm
10.3 mm
11.7 mm
13.1 mm

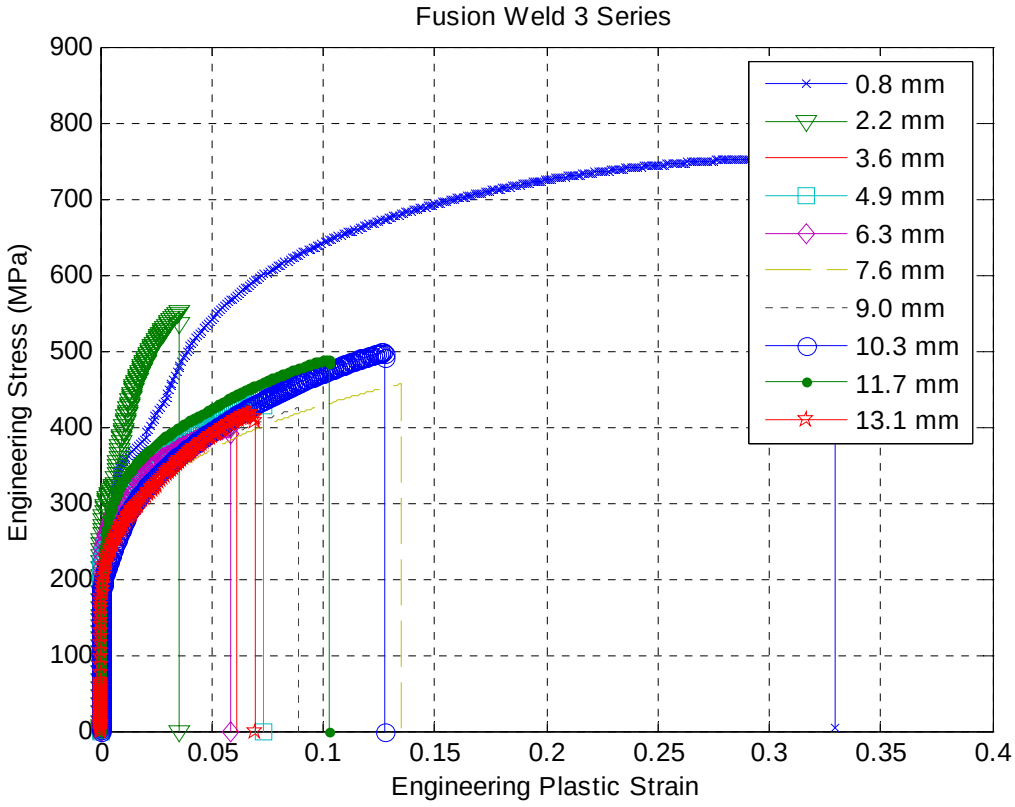
Fusion Weld 3 Series
Engineering Stress (MPa)
Engineering Plastic Strain
0.8 mm
2.2 mm
3.6 mm
4.9 mm
6.3 mm
7.6 mm
9.0 mm
10.3 mm
11.7 mm
13.1 mm

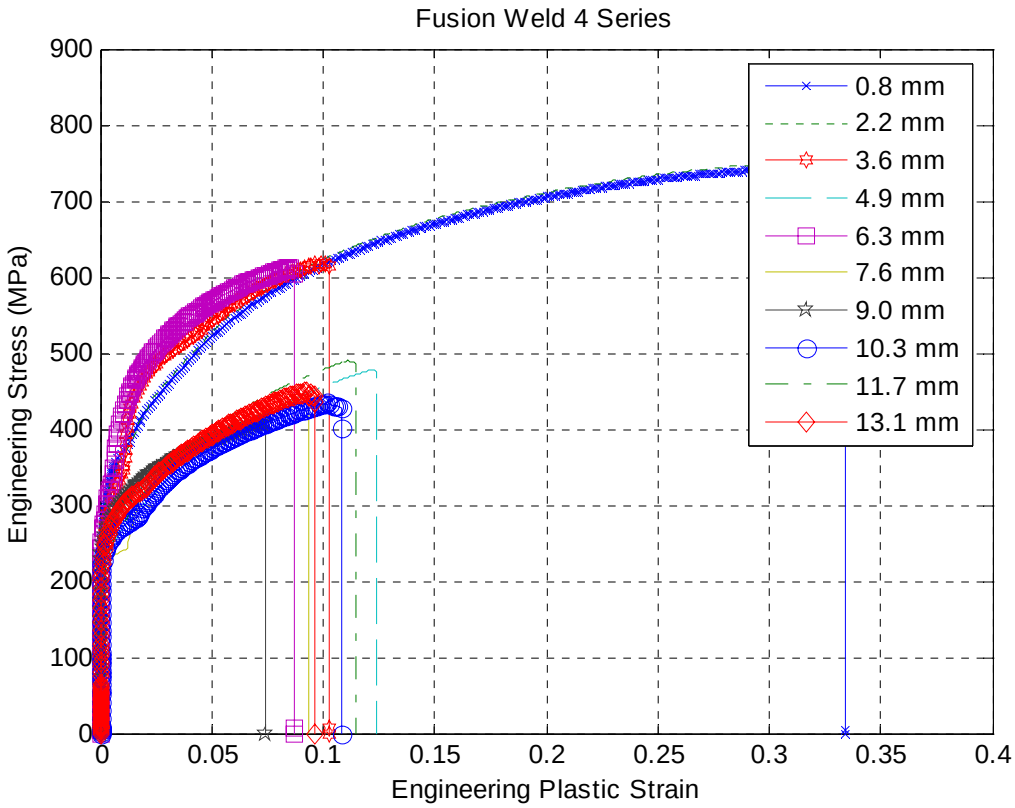
Fusion Weld 4 Series
Engineering Stress (MPa)
Engineering Plastic Strain
0.8 mm
2.2 mm
3.6 mm
4.9 mm
6.3 mm
7.6 mm
9.0 mm
10.3 mm
11.7 mm
13.1 mm

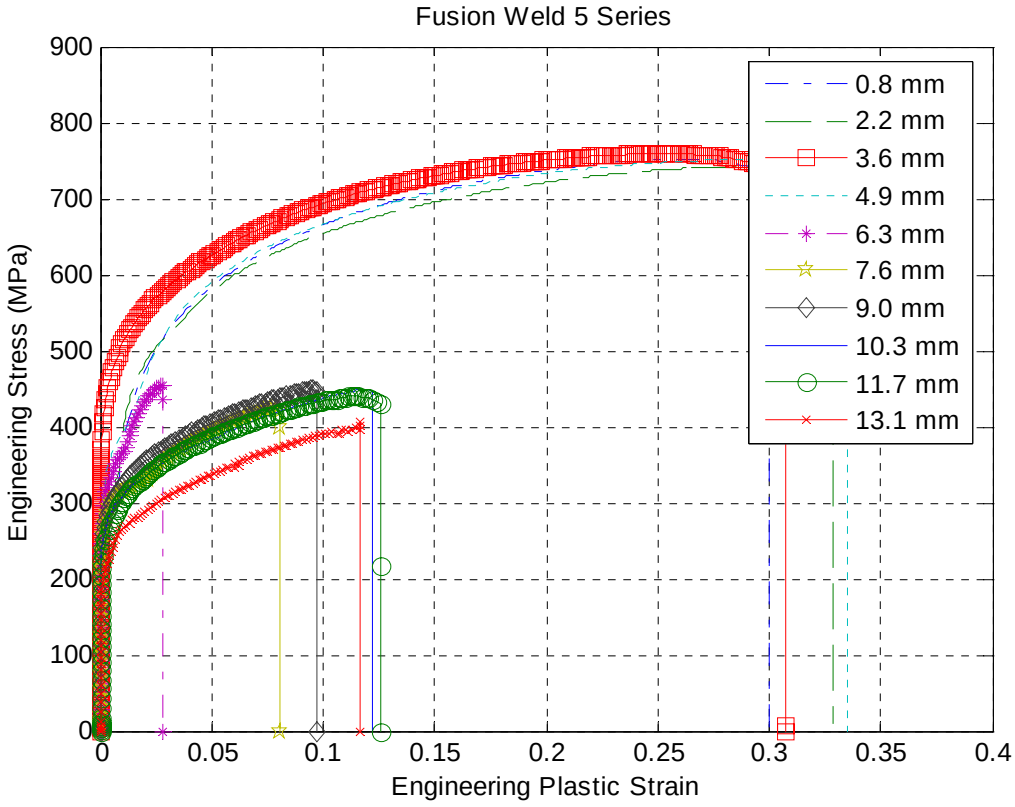
Fusion Weld 5 Series
Engineering Stress (MPa)
Engineering Plastic Strain
0.8 mm
2.2 mm
3.6 mm
4.9 mm
6.3 mm
7.6 mm
9.0 mm
10.3 mm
11.7 mm
13.1 mm

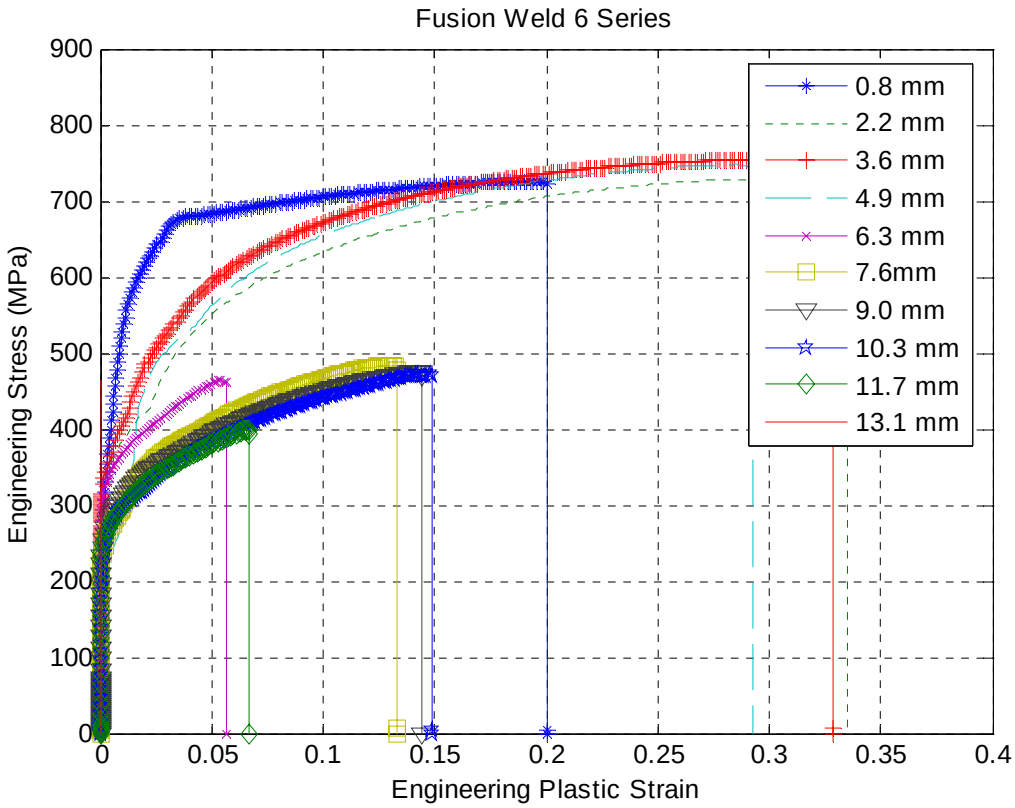
Fusion Weld 6 Series
Engineering Stress (MPa)
Engineering Plastic Strain
0.8 mm
2.2 mm
3.6 mm
4.9 mm
6.3 mm
7.6mm
9.0 mm
10.3 mm
11.7 mm
13.1 mm

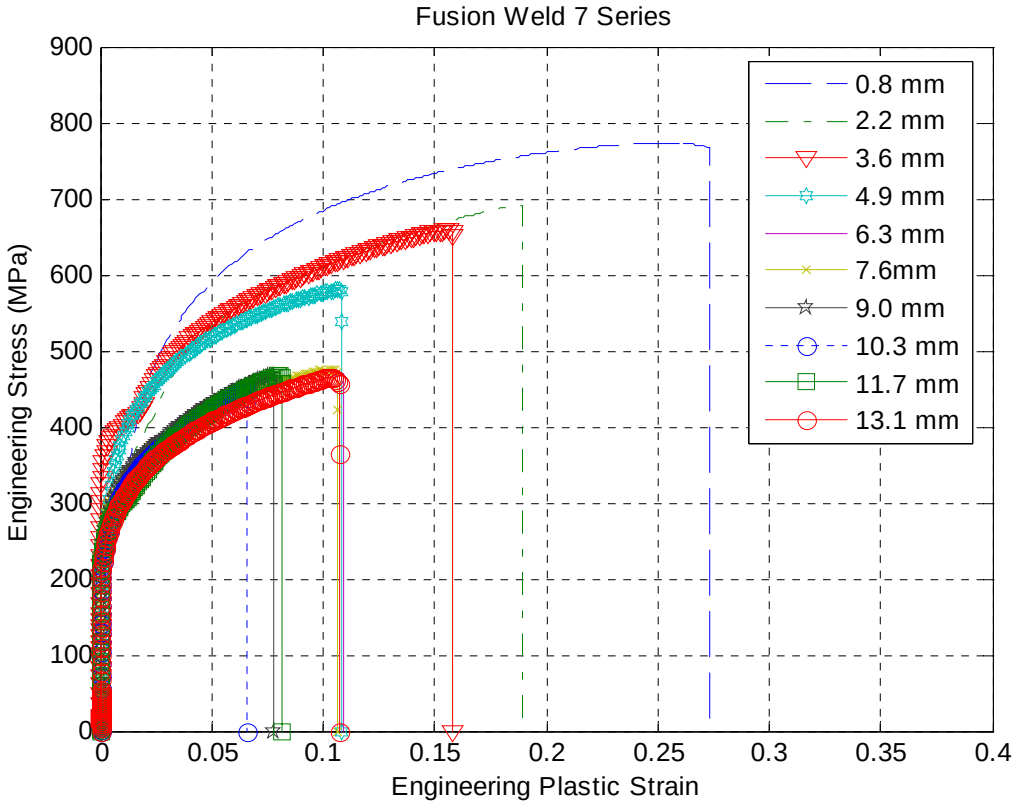
Fusion Weld 7 Series
Engineering Stress (MPa)
Engineering Plastic Strain
0.8 mm
2.2 mm
3.6 mm
4.9 mm
6.3 mm
7.6mm
9.0 mm
10.3 mm
11.7 mm
13.1 mm

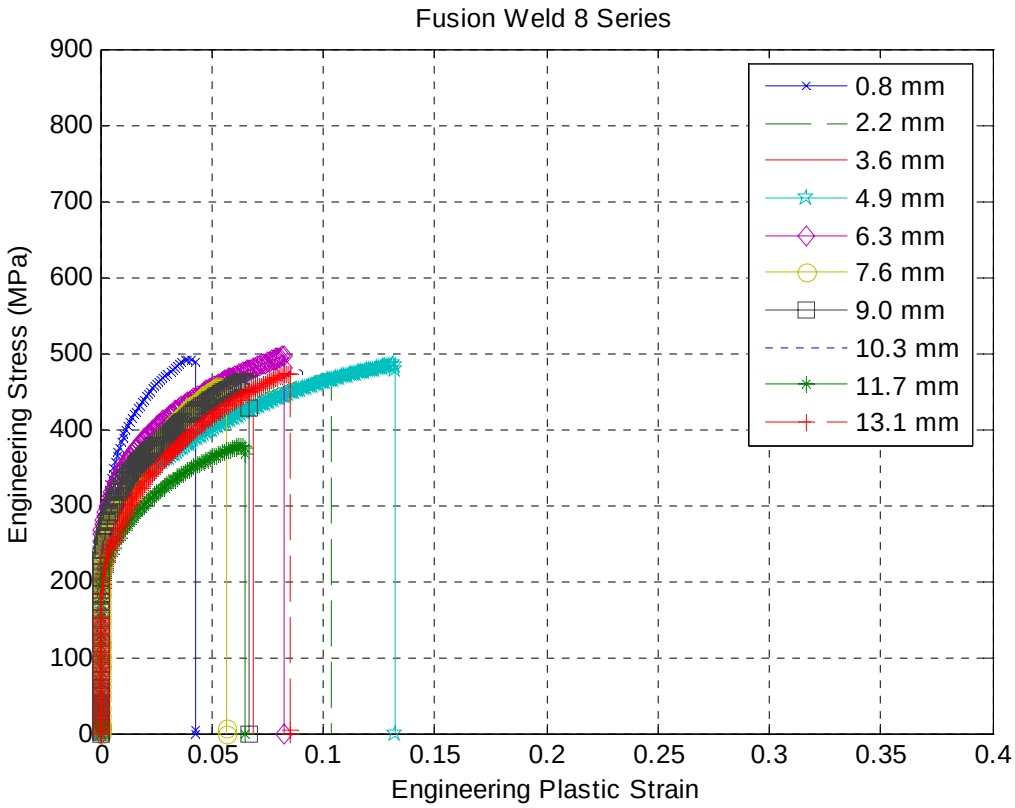
Fusion Weld 8 Series
Engineering Stress (MPa)
Engineering Plastic Strain
0.8 mm
2.2 mm
3.6 mm
4.9 mm
6.3 mm
7.6 mm
9.0 mm
10.3 mm
11.7 mm
13.1 mm

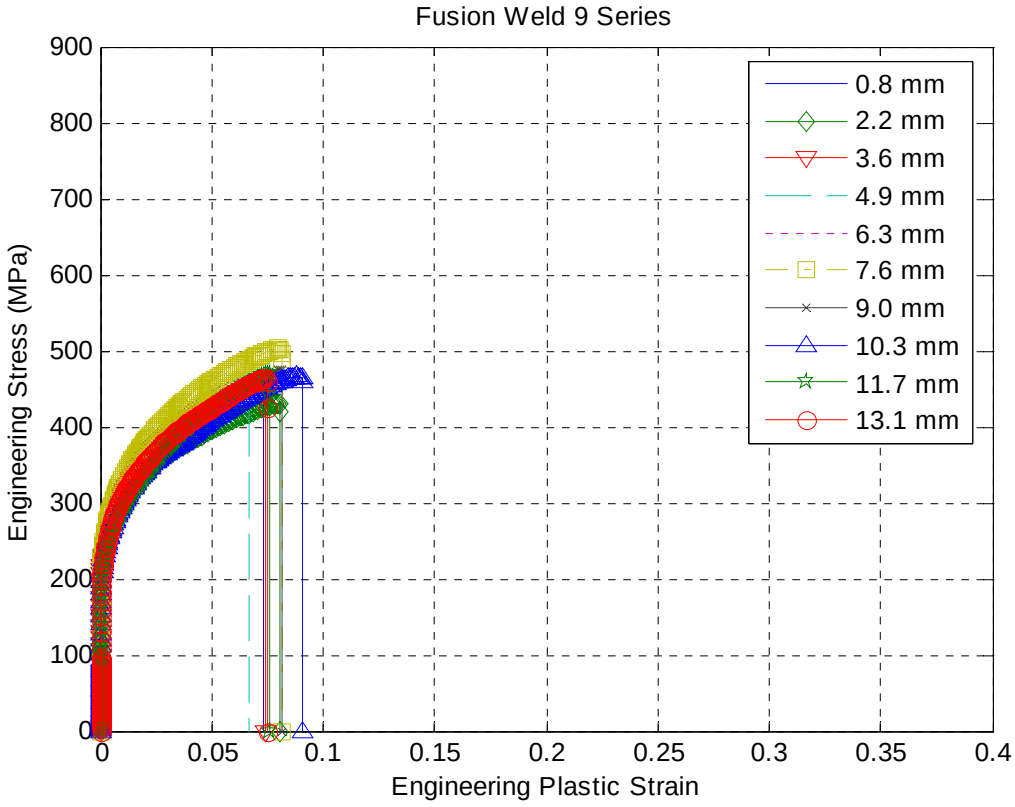
Fusion Weld 9 Series
Engineering Stress (MPa)
Engineering Plastic Strain
0.8 mm
2.2 mm
3.6 mm
4.9 mm
6.3 mm
7.6 mm
9.0 mm
10.3 mm
11.7 mm
13.1 mm

E. 1398 SERIES (LONGITUDINAL)

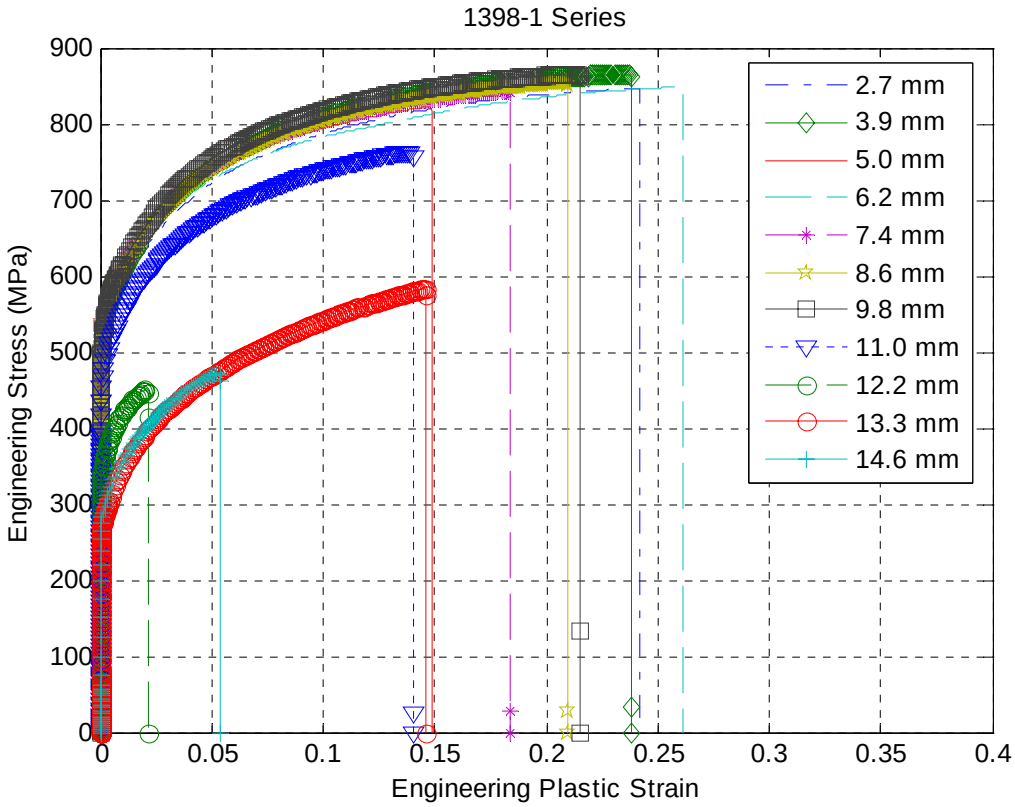

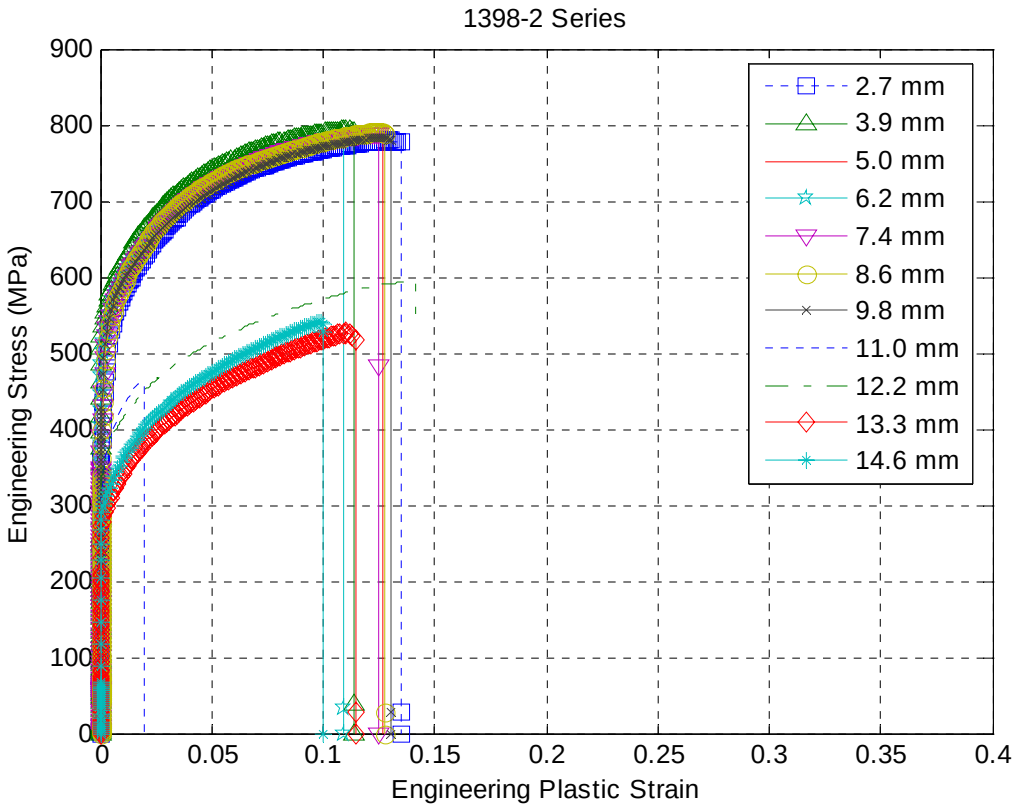
1398-2 Series
Engineering Stress (MPa)
Engineering Plastic Strain
2.7 mm
3.9 mm
5.0 mm
6.2 mm
7.4 mm
8.6 mm
9.8 mm
11.0 mm
12.2 mm
13.3 mm
14.6 mm

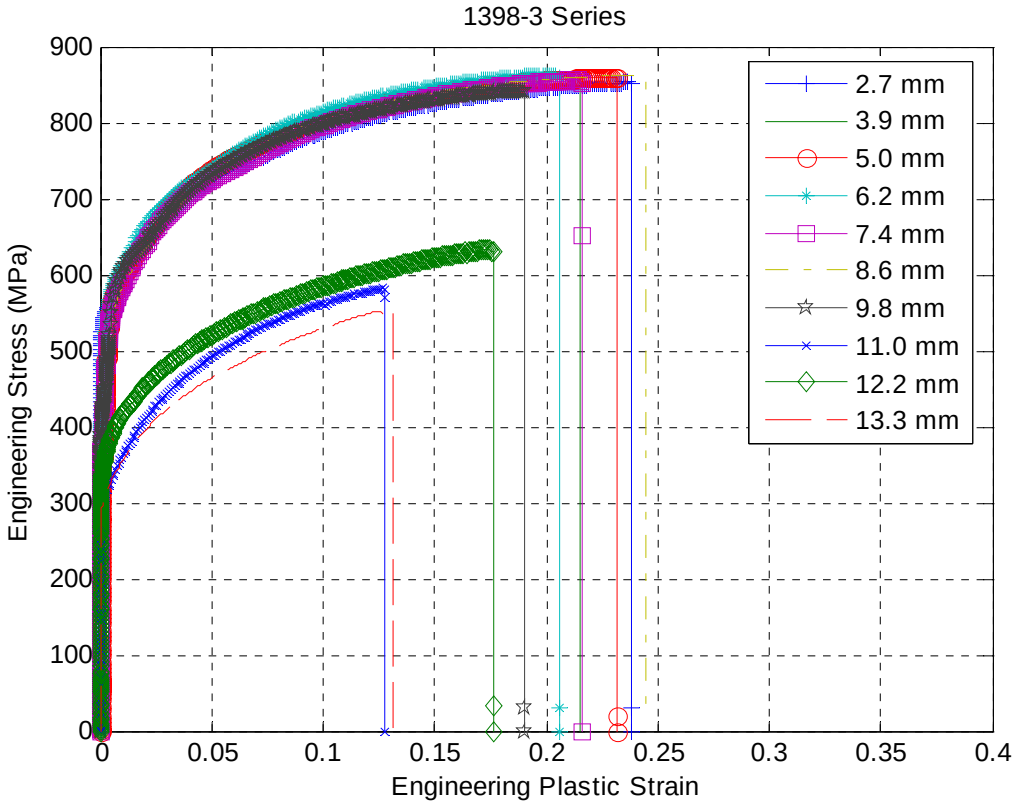
1398-3 Series
Engineering Stress (MPa)
Engineering Plastic Strain
2.7 mm
3.9 mm
5.0 mm
6.2 mm
7.4 mm
8.6 mm
9.8 mm
11.0 mm
12.2 mm
13.3 mm

F. 1398 SERIES (TRANSVERSE)

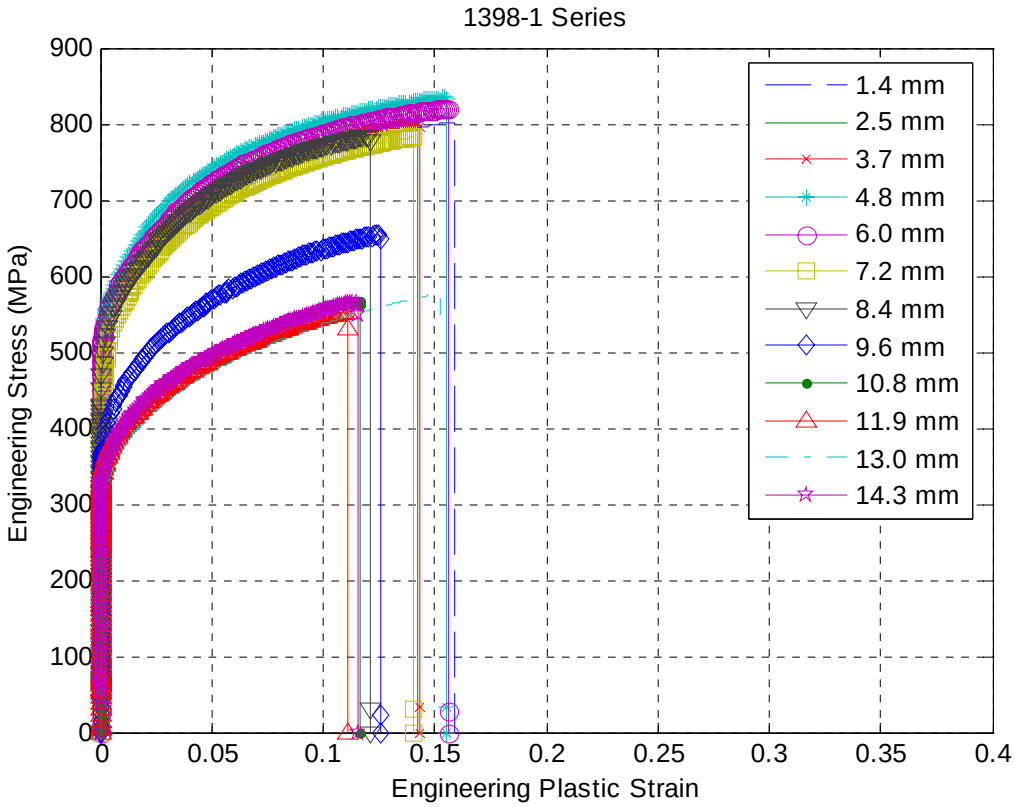

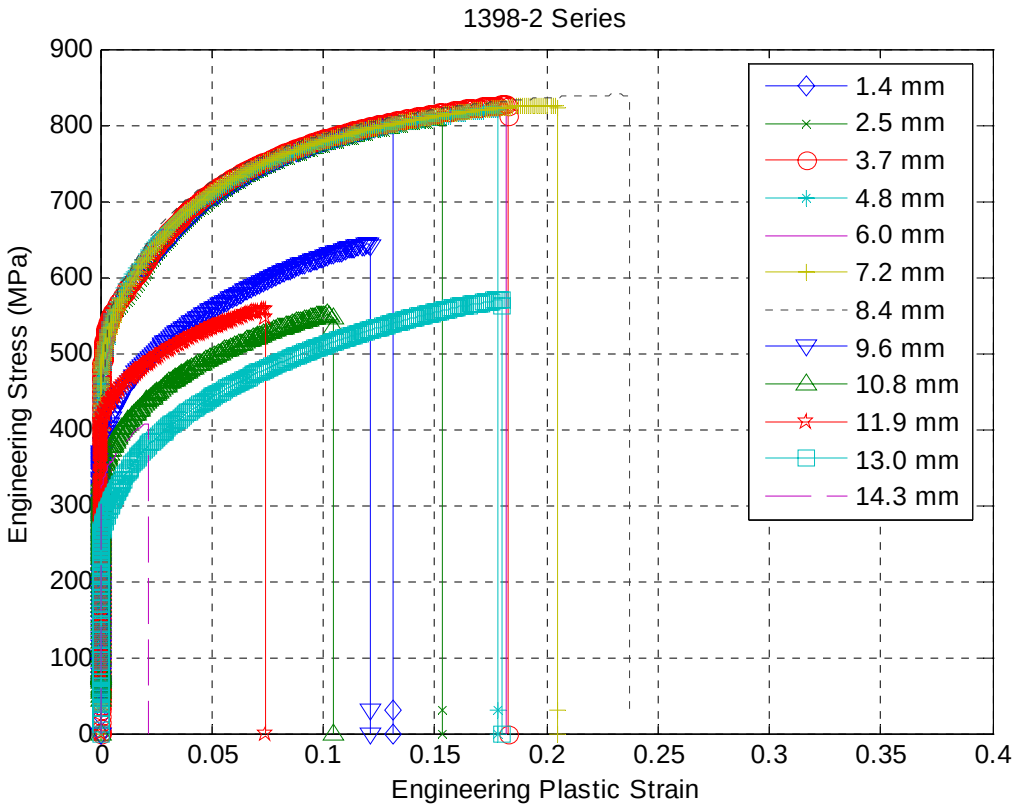
1398-2 Series
Engineering Stress (MPa)
Engineering Plastic Strain
0
100
200
300
400
500
600
700
800
900
0
0.05
0.1
0.15
0.2
0.25
0.3
0.35
0.4
1.4 mm
2.5 mm
3.7 mm
4.8 mm
6.0 mm
7.2 mm
8.4 mm
9.6 mm
10.8 mm
11.9 mm
13.0 mm
14.3 mm

THIS PAGE INTENTIONALLY LEFT BLANK

APPENDIX B – MESH PLOTS AND MECHANICAL PROPERTY DISTRIBUTIONS AS A FUNCTION OF DEPTH FOR 741 SERIES

A. LONGITUDINAL MESH PLOTS

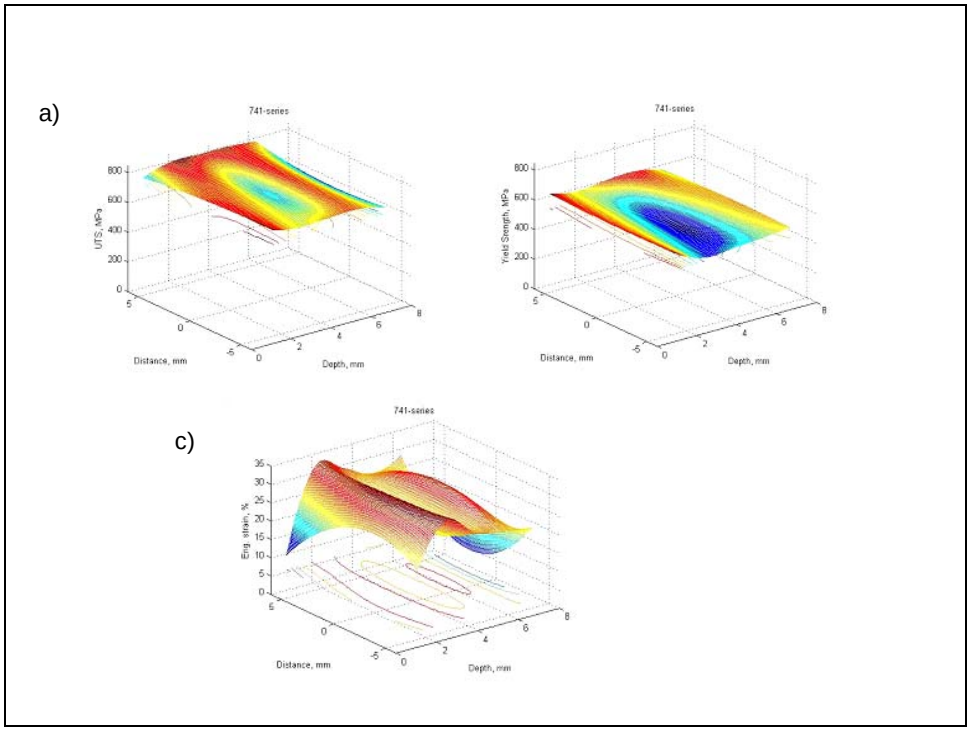

B. MECHANICAL PROPERTY DISTRIBUTIONS

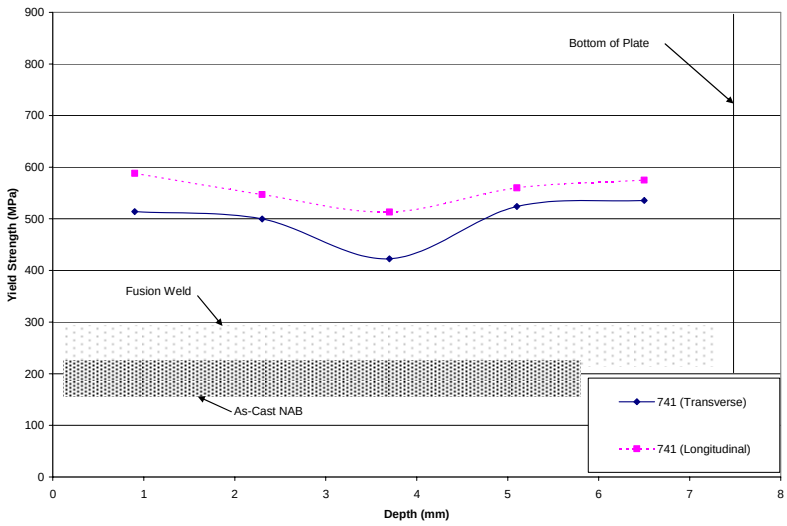

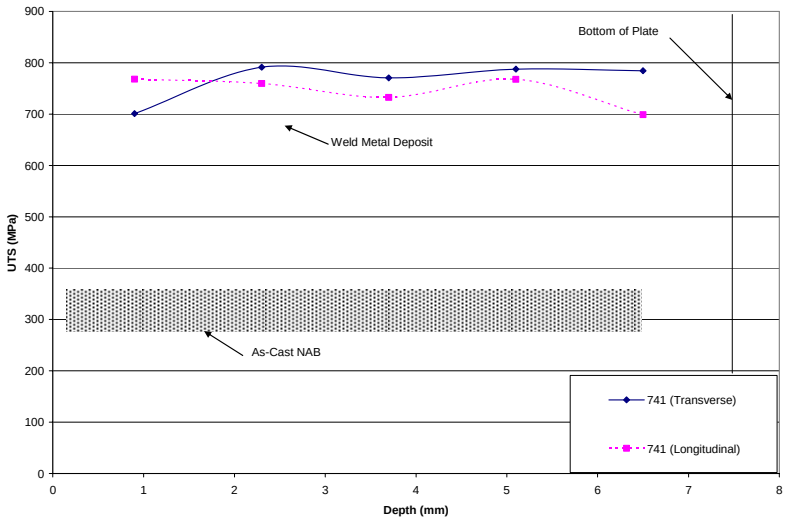
Bottom of Plate
Weld Metal Deposit
As-Cast NAB
741 (Transverse)
741 (Longitudinal)
UTS (MPa)
Depth (mm)
900
800
700
600
500
400
300
200
100
0
0
1
2
3
4
5
6
7
8

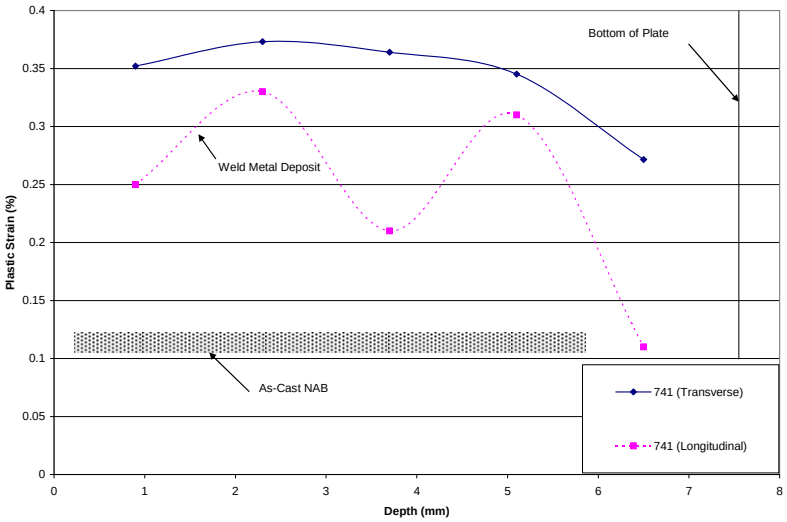
Bottom of Plate
Weld Metal Deposit
As-Cast NAB
741 (Transverse)
741 (Longitudinal)
Plastic Strain (%)
Depth (mm)
0.4
0.35
0.3
0.25
0.2
0.15
0.1
0.05
0
0
1
2
3
4
5
6
7
8

APPENDIX C– SELECTED MICROGRAPHS AND FRACTURE SURFACES FOR 740, 741 AND 751 FSP SERIES

A. 740 SERIES (TRANSVERSE)

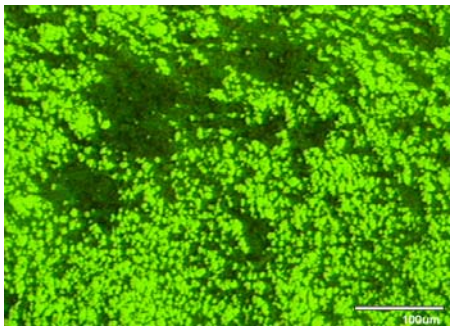
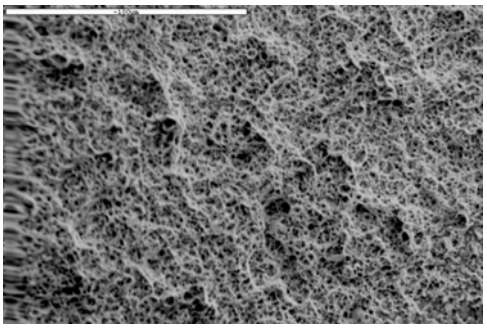

Top of 740 (740-1-1)

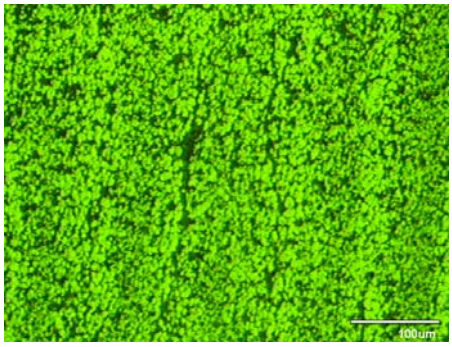
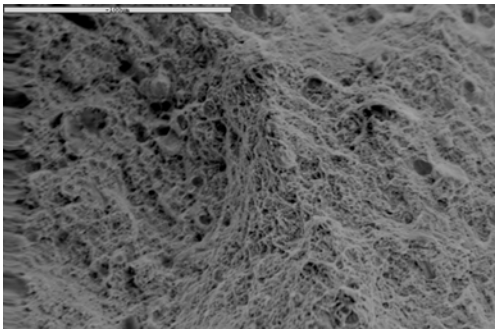

Middle of 740(740-1-3)

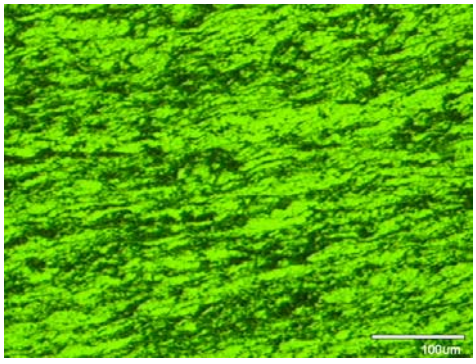
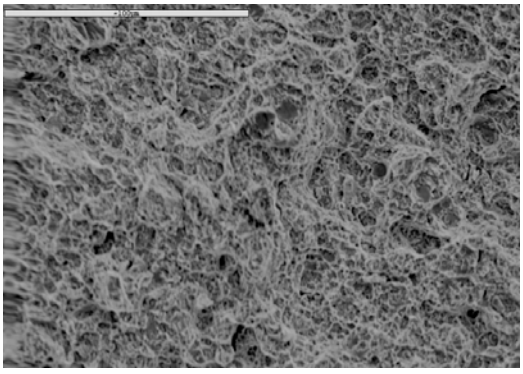

Bottom of 740 (740-1-5)

B. 741 SERIES (TRANSVERSE)

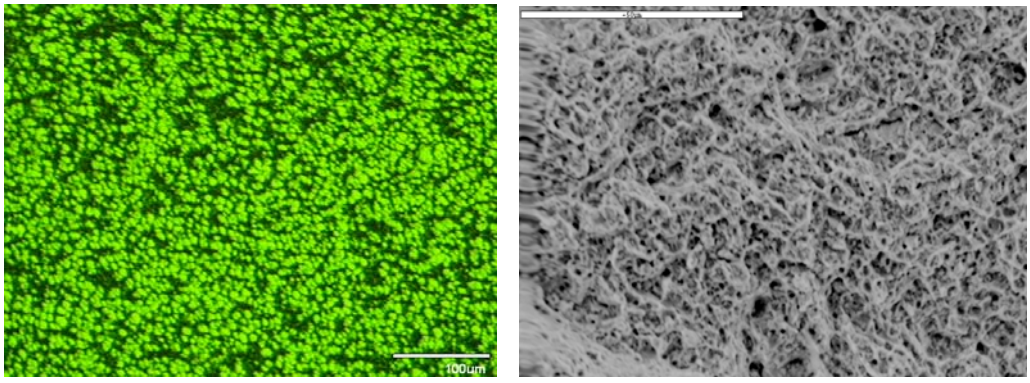

Top of 741 (741-1-1)

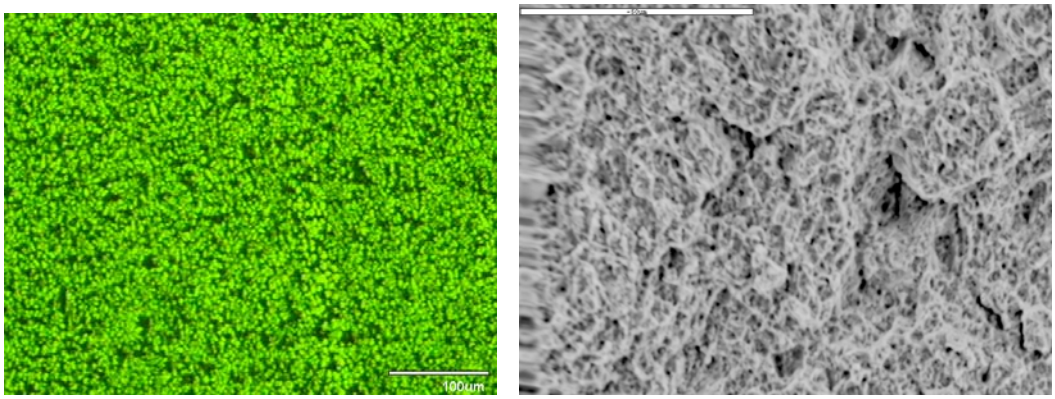

Middle of 741 (741-1-3)

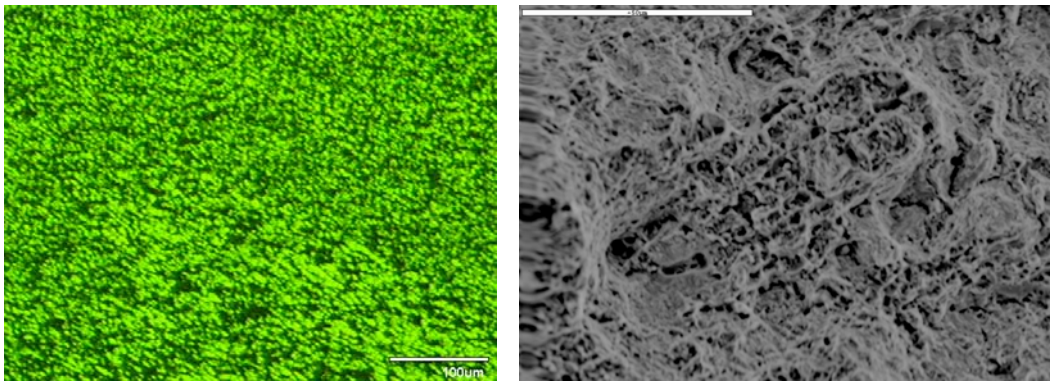

Bottom of 741 (741-1-5)

C. 751 SERIES (TRANSVERSE)

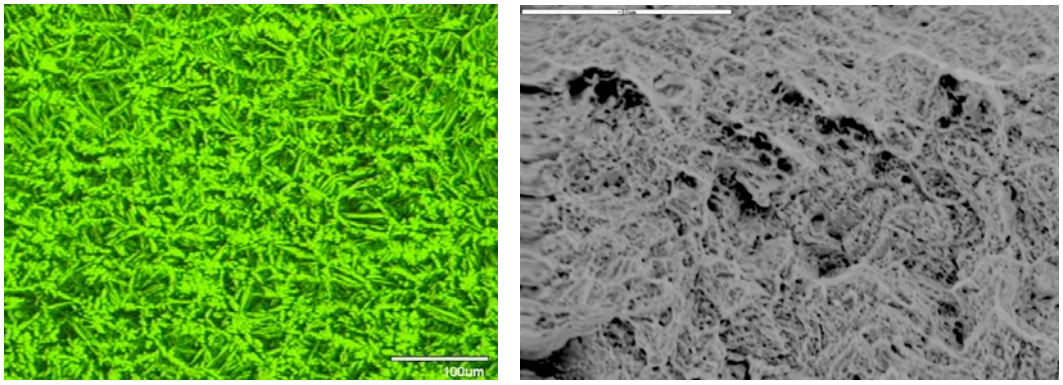

Top of 751 (751-1-1)

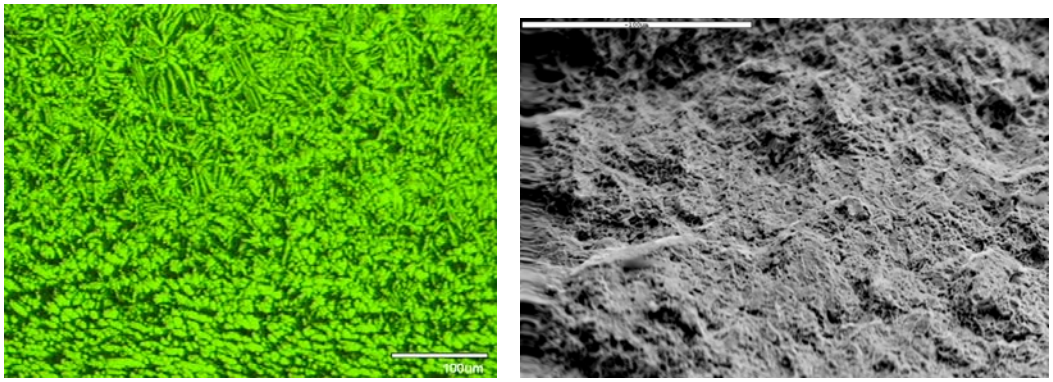

Middle of 751 (751-1-3)

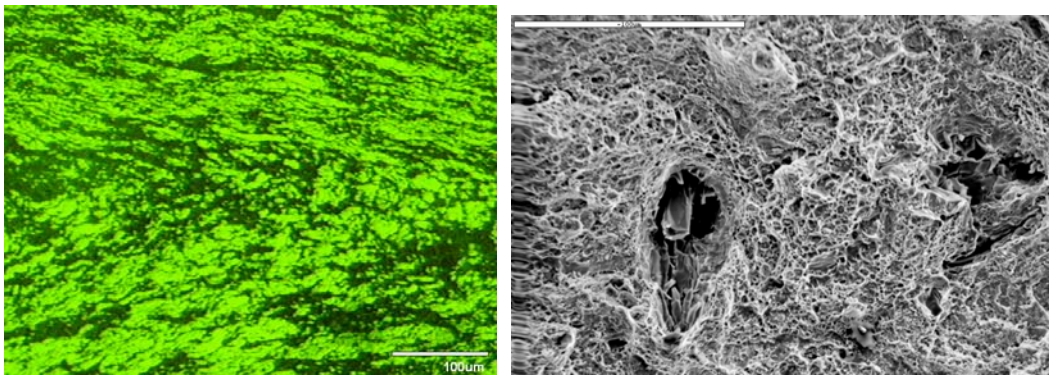

Bottom of 751 (751-1-5)

THIS PAGE INTENTIONALLY LEFT BLANK

APPENDIX D – TABLES

A. 740, 741 AND 751 SERIES (TRANSVERSE)

		740 (Yield Strength(MPa))	
	Blank 1	Blank 2	Blank 3
1	575.74	513.78	512.97
2	590.16	484.09	520.32
3	569.77	502.44	503.16
4	569.7	556.42	537.11
5	591.08	485.19	565.13
		741 (Yield Strength(MPa))	
	Blank 1	Blank 2	Blank 3
1	481.97	474.73	585.08
2	504.43	505.89	489.1
3	427.61	442.17	397.86
4	518.8	590.66	461.92
5	578.65	599.83	428.12
		751 (Yield Strength(MPa))	
	Blank 1	Blank 2	Blank 3
1	485.37	507.04	595.35
2	530.98	720.99	518.63
3	473.32	530.87	439.47
4	498.03	436.9	423.83
5	585.1	610.35	465.36

		740 (UTS (MPa))	
	Blank 1	Blank 2	Blank 3
1	736.41	711.67	763.9
2	735.45	705.09	749.64
3	815.96	749.37	747.48
4	818.33	752.73	780.87
5	788.1	734.18	701.33
		741 (UTS(MPa))	
	Blank 1	Blank 2	Blank 3
1	784.56	594.5	724.24
2	763.29	836.39	775.08
3	771.22	778.13	762.74
4	787.26	792.14	783.77
5	782.59	809.68	761.91
		751 (UTS(MPa))	
	Blank 1	Blank 2	Blank 3
1	809.22	818	818.39
2	793.44	745.34	801.21
3	786.86	807.71	804.4
4	832.13	830.04	813.27
5	730.99	788.74	769.54

		740 (Elongation(%))	
	Blank 1	Blank 2	Blank 3
1	0.0828	0.1408	0.2447
2	0.0859	0.1689	**0.05**
3	0.172	0.2097	0.1843
4	0.1934	0.2162	0.2413
5	0.1703	0.2051	0.1311
		741 (Elongation(%))	
	Blank 1	Blank 2	Blank 3
1	0.3521	**0.0746**	**0.1289**
2	0.3328	0.388	0.3989
3	0.3805	0.3772	**0.3344**
4	0.3396	0.3059	0.3901
5	0.275	0.2806	**0.2593**
		751 (Elongation(%))	
	Blank 1	Blank 2	Blank 3
1	0.254	0.2657	0.2299
2	0.287	**0.22**	0.2827
3	0.308	0.3021	0.3519
4	0.3052	**0.1991**	0.3512
5	0.0825	0.1311	0.1624

B. FUSION WELD (LONGITUDINAL)

		Fusion Weld Yield Strength (MPa)							
	1	2	3	4	5	6	7	8	9
1	197.93	208.13	244.75	281.44	214.78	228.23	279.69	173.89	233.38
2	217.19	216.49	231.46	271.01	256.03	293.1	218.81	234.33	230.15
3	189.17	221.26	214.46	227.04	216.95	207.18	167.25	193.54	157.15
4	226.43	158.16	202.31	204.57	282.08	188.49	206.1	230.52	197.64
5	197.21	225.08	158.91	260.79	284.81	209.74	240.03	194.04	200.65
6	154.11	193.85	205.33	205.5	134.5	213.6	250.04	186.17	207.14
7	130.55	172.72	200.43	197.12	240.19	254.23	227.06	220.32	199.23
8	168.14	200.06	199.27	215.44	216.59	244.68	202.58	224.19	209.11
9	168.6	175.65	208.58	195.08	204.33	223.96	197.85	185.36	192.52
10	152.76	148.1	174.62	221.84	171.29	229.05	214.98	221.73	176.67

		Fusion Weld UTS (MPa)							
	1	2	3	4	5	6	7	8	9
1	309.74	385.89	748.23	742.26	728.03	721.21	766.34	488.47	470.51
2	476.86	430	552.4	747.68	728.12	717.15	690.5	467.33	429.62
3	412.83	456.21	419.26	613.55	724.15	740.45	657.57	429.18	452.7
4	604.81	425.68	437.92	475.12	734.23	739.04	578.45	482.91	430.12
5	463.45	464.94	397.64	604.84	453.84	461.43	469.5	495.17	468.34
6	286.68	453.92	455.28	441.38	420.25	478.16	473.28	447.49	496.86
7	226	435.63	424.09	408.47	446.66	475.52	467.31	460.14	473.95
8	369.68	423.9	496.94	428.13	446.36	470.1	445.54	474.15	464.65
9	440.4	445.14	489.24	485.28	429.65	398.89	464.73	375.75	470.47
10	390.46	339.51	412.57	442.25	406.77	443.34	456.46	471.35	460.38

		Fusion Weld Elongation (%)							
	1	2	3	4	5	6	7	8	9
1	0.0295	0.0233	0.3296	0.3345	0.3	0.2006	0.2735	0.0424	0.0731
2	0.1108	0.0699	0.0357	0.3489	0.3288	0.3346	0.1898	0.1034	0.0803
3	0.0667	0.1028	0.0608	0.1031	0.307	0.3283	0.1579	0.069	0.0746
4	0.0993	0.0771	0.0729	0.1238	0.3346	0.293	0.1085	0.1321	0.0664
5	0.1217	0.0959	0.0587	0.0866	0.0281	0.0569	0.1091	0.0824	0.0888
6	0.0671	0.1229	0.1347	0.0932	0.0804	0.1336	0.1067	0.0565	0.0815
7	0.0342	0.1238	0.0893	0.0745	0.0976	0.1446	0.0783	0.0667	0.0812
8	0.105	0.1331	0.1275	0.1079	0.1219	0.1491	0.0657	0.0907	0.0906
9	0.1037	0.1309	0.1029	0.1149	0.1257	0.0667	0.0815	0.0651	0.0761
10	0.0996	0.0493	0.0697	0.0959	0.1166	0	0.1074	0.0853	0.0747

C. 1398 SERIES

1. Longitudinal

		1398 Yield Strength (MPa)	
	1	2	3
1	627.24	623.49	632.79
2	644.88	656.74	657.26
3	650.27	636.93	641.19
4	542.36	636.7	655.59
5	656.67	633.64	633.03
6	646.8	636.7	627.66
7	658.57	631.12	635.38
8	593.21	458.75	402.26
9	448.13	446.93	447.89
10	385.93	376.26	390.56
11	393.51	396.4	395

		1398 UTS (MPa)	
	1	2	3
1	845.02	777.63	852.41
2	862.05	790.68	862.8
3	816.75	781.07	858.78
4	848.01	777.29	858.76
5	841.66	787.58	850.95
6	850.92	788.12	857.79
7	862.57	799.64	840.69
8	757.3	459.86	579.66
9	447.01	594.32	629.99
10	582.56	516.5	555.2
11	470.64	538.27	505

		1398 Elongation (%)	
	1	2	3
1	0.2421	0.1347	0.2379
2	0.2383	0.1137	0.2149
3	0.1486	0.1264	0.2315
4	0.2706	0.1091	0.2057
5	0.1836	0.1251	0.2163
6	0.2097	0.1281	0.2443
7	0.2156	0.1306	0.1904
8	0.1401	0.0197	0.1274
9	0.0217	0.1413	0.1769
10	0.1461	0.1143	0.1315
11	0.0536	0.0999	**0**

2. Transverse

		1398 Yield Strength (MPa)
	1	2
1	607.59	605.39
2	633.1	592.14
3	625.81	612.86
4	652.72	622.02
5	631.6	620
6	600.87	614.86
7	615.95	635.1
8	488.22	480.15
9	429.68	429.91
10	426.25	480.55
11	404.91	369.81
12	430.4	404.23

		1398 UTS (MPa)
	1	2
1	801.09	802.1
2	828.04	803.1
3	796.03	826.09
4	834.07	819.18
5	820.32	822.53
6	782.03	826.38
7	778.18	838.34
8	649.52	641.75
9	567.94	545.53
10	550.7	555.78
11	575.5	568.45
12	561.44	407.07

		1398 Elongation (%)
	1	2
1	0.1594	0.1311
2	0.1422	0.1533
3	0.1431	0.1833
4	0.1553	0.1782
5	0.1567	0.1817
6	0.1404	0.205
7	0.1215	0.237
8	0.1262	0.1212
9	0.1166	0.1046
10	0.1108	0.0743
11	0.1529	0.1806
12	0.116	0.0213

LIST OF REFERENCES

1. Mishra, R.S., *Advanced Materials and Processes, v.* 161(10), pp. 43-46, 2003.

2. Mishra, R.S., Ma Z.Y., and Charit, I., *Mater. Sci. Engineering A, v.* A341, pp. 30710, 2003.

3. Ma, Z.Y., Mishra, R.S., and Mahoney, M. W., "Friction Stir Welding and Processing II", K.V. Jata, M.W. Mahoney, R.S. Mishra, S.L. Semiatin and T. Lienert, eds., TMS, Warrendale, PA, pp. 221-30, 2003.

4. W. M. Thomas et. al., "Friction Stir Butt Welding", International Patent Appl. No. PCT/GB92/02203 and GB Patent Appl. No. 9125978.8, Dec 1991, U.S. Patent No. 5,460,317 – from [Ref. 2] in support of information by Stephan Kallee and David Nicholas, TWI.

5. Rhodes, C. G. et al., "Effects of Friction Stir Welding on Microstructure of 7075 Aluminum," *Scripta Materialia, v.* 36, No. 1, p. 69-75, 1997.

6. Jata, K.V. and Semiatin, S.L, "Continuous Dynamic Recrystallization During Friction Stir Welding of High Strength Aluminum Alloys," *Scripta Materialia, v.* 43, p. 743-749, 2000.

7. Mishra, R.S. and Mahoney, M.W., "Friction Stir Processing: A New Grain Refinement Technique to Achieve High Strain Rate Superplasticity in Commercial Alloys," *Materials Science Forum, v*. 357-359, p. 507-514, 2001.

8. Williams, R. A., MS Thesis, "A Microstructural and Mechanical Property Correlation of Friction Stir Processed Nickel Aluminum Bronze," Naval Postgraduate School, Monterey, CA, Sep 2004.

9. Sahoo, M., "Structure and Mechanical Properties of Slow-Cooled Nickel-Aluminum Bronze Alloy C95800," *AFS Trans, v*. 90, p. 913-926, 1982.

10. Culpan, E.A. and Rose, G., "Corrosion Behaviour of Cast Nickel Aluminium Bronze in Sea Water," *British Corrosion Journal, v.* 14, p. 160-166, 1979.

11. American Society for Testing and Materials (ASTM) B148 – 93a, Standard Specification for Aluminum-Bronze Sand Castings.

12. Sahoo, M., "Weldability of Nickel-Aluminum Bronze Alloy C95800," *AFS Trans,* v. 112, p. 893-911, 1982.

13. Wenschot, P., "The Properties of Ni-Al Bronze Sand Cast Ship Propellers in Relation to Section Thickness," *International Shipbuilding Progress*, v. 34, p.112-123, 1987.

14. Mahoney M. W., Bingel W. H., and Mishra R. S., "Microstructural Modification and Resultant Properties of Friction Stir Processed Cast NiAl Bronze" DARPA sponsored FSP website "Presentations and Publications."

http://www.darpa.mil/dso/thrust/matdev/fsp/prespub.html
Last access: 17 May 05

15. Oh-Ishi, K. and McNelley, T., "Microstructural Modification of As-Cast NiAl Bronze by Friction Stir Processing" *Metallurgical and Materials Transactions, v.* 35A, p. 2951-2960, 2004.

16. Oh-Ishi, K. and McNelley, T., "The Influence of Friction Stir Processing Parameters on Microstructure of As-Cast NiAl Bronze" *Metallurgical and Materials Transactions, v.* 36A, p. 1575-1585, 2005.

17. Pierce, F. A., MS Thesis, "The Isothermal Deformation of Nickel-Aluminum Bronze in Relation to the Friction Stir Processing," Naval Postgraduate School, Monterey, CA, Jun 2004.

18. American Society for Testing and Materials (ASTM) E-8, Standard Test Methods for Tension Testing of Metallic Materials.

19. Mahoney, M. W., Rockwell Scientific Corporation, private communication, February 2005.

20. Nguyen, J., Naval Surface Warfare Center, Carderock Div., private communication, February 2005.

21. Metals Handbook, 9th Ed., v. 2, Properties & Selections: Nonferrous Alloys and Pure Metals.

INITIAL DISTRIBUTION LIST

1. Defense Technical Information Center
   Ft. Belvoir, Virginia

2. Dudley Knox Library
   Naval Postgraduate School
   Monterey, California

3. Professor Terry McNelley
   Naval Postgraduate School
   Dept. of Mechanical Engineering
   Monterey, California

4. Professor A. J. Healey
   Naval Postgraduate School
   Dept. of Mechanical Engineering
   Monterey, California

5. CDR W. Plott
   Naval Postgraduate School
   Dept. of Mechanical Engineering
   Monterey, California

6. Murray W. Mahoney
   Rockwell Scientific Center
   Thousand Oaks, California

7. William Palko
   Naval Surface Warfare Center
   Carderock Division
   West Bethesda, Maryland

8. Dr. Leo Christodoulou
   DARPA/DSO
   Arlington, VA